molecules

MDPI

Review

Recent Advances in *bis*-Chalcone-Based Photoinitiators of Polymerization: From Mechanistic Investigations to Applications

Nicolas Giacoletto * and Frédéric Dumur *

Aix Marseille Univ, CNRS, ICR UMR 7273, F-13397 Marseille, France

* Correspondence: nicolas.giacoletto@etu.univ-amu.fr or nicolasgiacoletto@gmail.com (N.G.); frederic.dumur@univ-amu.fr (F.D.)

Abstract: Over the past several decades, photopolymerization has become an active research field, and the ongoing efforts to develop new photoinitiating systems are supported by the different applications in which this polymerization technique is involved—including dentistry, 3D and 4D printing, adhesives, and laser writing. In the search for new structures, *bis*-chalcones that combine two chalcones' moieties within a unique structure were determined as being promising photosensitizers to initiate both the free-radical polymerization of acrylates and the cationic polymerization of epoxides. In this review, an overview of the different *bis*-chalcones reported to date is provided. Parallel to the mechanistic investigations aiming at elucidating the polymerization mechanisms, *bis*-chalcones-based photoinitiating systems were used for different applications, which are detailed in this review.

Keywords: chalcone; ketone; photopolymerization; photosensitizers; Claisen-Schmidt condensation

Citation: Giacoletto, N.; Dumur, F. Recent Advances in *bis*-Chalcone-Based Photoinitiators of Polymerization: From Mechanistic Investigations to Applications. *Molecules* **2021**, *26*, 3192. https://doi.org/10.3390/molecules26113192

Academic Editor: Teobald Kupka

Received: 1 May 2021
Accepted: 23 May 2021
Published: 26 May 2021

1. Introduction

Polymerization consists of converting a liquid resin into a solid, and different approaches can be used to obtain this result. As the most popular approach, the polymerization can be instigated by heat, and for this purpose, various thermal polymerization techniques have been developed over the years—such as ring-opening polymerization (ROP) [1,2], reversible addition–fragmentation chain-transfer (RAFT) polymerization [3], and nitroxide-mediated polymerization (NMP) [4–6]. Parallel to this, light can also be used to generate initiating species. While, historically, photopolymerization was mostly based on UV photoinitiating systems, UV light is now the focus of numerous safety concerns, such that a great deal of effort is now being devoted to developing visible light photoinitiating systems offering safer working conditions for the operator (no skin or eye damage) [7–16]. Furthermore, improved light penetration can be achieved in the visible range compared to that obtained with UV light, as shown in Figure 1. Indeed, if light penetration remains limited in the UV range (600 µm), a major improvement can be achieved with visible light, which can range between 4 mm and 5 cm, depending on the irradiation wavelength [17]. As a result of this, the scope of application of photopolymerization has been totally revolutionized, since the use of near-infrared light now allows for the polymerization of thick and filled samples, which is not achievable with UV photoinitiating systems [18–20]. The development of visible light photoinitiating systems is also supported by the easy access to cheap, compact, lightweight, and energy-saving irradiation sources such as light-emitting diodes (LEDs) [21,22]. Faced with this easy availability of LEDs with tunable irradiation wavelengths, the demand for photopolymerizable resins activable at these different wavelengths has similarly increased. In particular, numerous photoinitiating systems activable at 405 nm have been developed over the last several years—this wavelength being the wavelength currently in use for 3D printers [23–28]. Interest in photopolymerization is also supported by the different advantages this polymerization technique offers compared to traditional thermal polymerization, which can only be realized in solution. Thus, photopolymerization can be carried out in solvent-free conditions so that the release of volatile organic

compounds (VOCs) can be advantageously avoided [29–32]. Natural compounds, photoinitiators, and monomers issued from renewable resources can also be used to elaborate photoinitiating systems and polymers, addressing the environmental impact and the toxicity issues raised by photopolymerization, and by polymerization more generally [33]. A spatial and a temporal control can also be obtained, meaning that the polymerization occurs only during the time the light is switched on, and only in the irradiated area (see Figure 2) [34,35]. The polymerization process can also be extremely fast, since it can be ended within a few seconds. This specificity is notably used advantageously with photopolymerizable glues and dental adhesives.

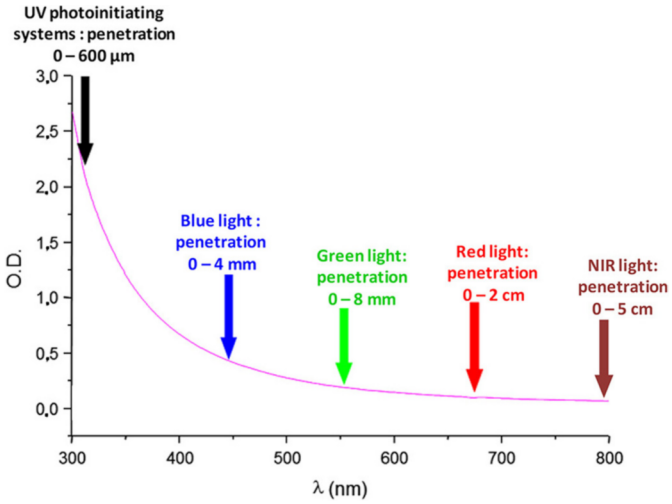

Figure 1. Light penetration in polystyrene latex with an average diameter of 112 nm. Reprinted with permission from Bonardi et al. [17]. Copyright 2018 American Chemical Society.

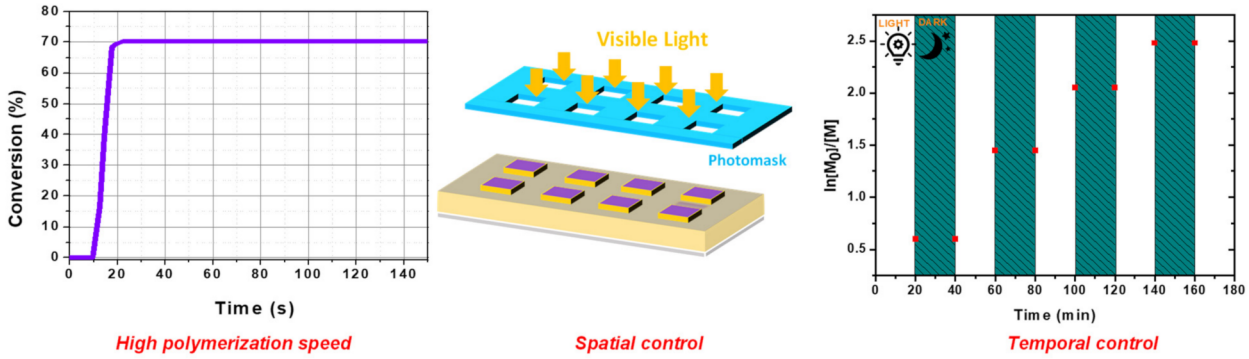

Figure 2. The different advantages of photopolymerization compared to traditional thermal polymerization.

Considering that visible light photopolymerization can be activated between 400 and 800 nm, numerous dyes absorbing in the visible range have been proposed, as exemplified with acridine-1,8-diones [36–38], carbazoles [39–44], pyrenes [45–50], iridium complexes, [51–59], copper complexes [60–70], squaraines [71–73], camphorquinones [74,75], perylenes [76–78], iodonium salts [79–81], benzophenones [82–87], cyanines [88,89], diketopyrrolopyrroles [90–92], helicenes [93,94], naphthalimides [95–107], chalcones [108–114], iron complexes [115–120], chromones [121–123], thioxanthones [124–127], dihydroanthraquinones [128], porphyrins [129,130], zinc complexes [131], acridones [132,133], push–pull dyes [134–145], phenothiazines [146], coumarins [147–153], flavones [154], 2,3-diphenylquinoxaline derivatives [155], and cyclohexanones [156–159]. With the aim of generating initiating species, two distinct families of photoinitiators can be distinguished: The first family, type I photoinitiators, consists of molecules that can be photochemically cleaved upon excitation. The advantage of this strategy is that only a single component is nec-

essary to generate the initiating radicals, so the migratability of potential side products within the polymer is considerably reduced. As shown in Figure 3 with 2,2-dimethoxy-1,2-diphenylethan-1-one, upon photoexcitation, a methoxybenzyl and a benzoyl radical are simultaneously formed, improving the efficiency of the initiating step. Additionally, the two radicals can be connected to the polymer chain under growth so that no migratable residue remains within the polymer network, addressing the potential toxicity issue of the photoinitiating systems. However, while this approach is appealing, the availability of visible Type I photoinitiators remains limited, and most of the benchmark Type I photoinitiators are UV photoinitiators [160–162]. As a drawback, Type I photoinitiators are irreversibly consumed during the polymerization process, and so the concentration of radicals irreversibly decreases over time. Conversely, Type II photoinitiators are typically dyes absorbing in the visible range, which act as photosensitizers for UV photoinitiators. Upon photoinduced electron transfer from the excited photosensitizer towards the UV photoinitiator, initiating radicals can be generated [163]. As the most widely used UV photoinitiators, onium salts, and notably iodonium salts, which are easily accessible from various commercial sources can be cited as relevant examples [164–167]. Considering that dyes act as photosensitizers for UV photoinitiators, two-component or three-component photoinitiating systems are typically developed with Type II photoinitiators.

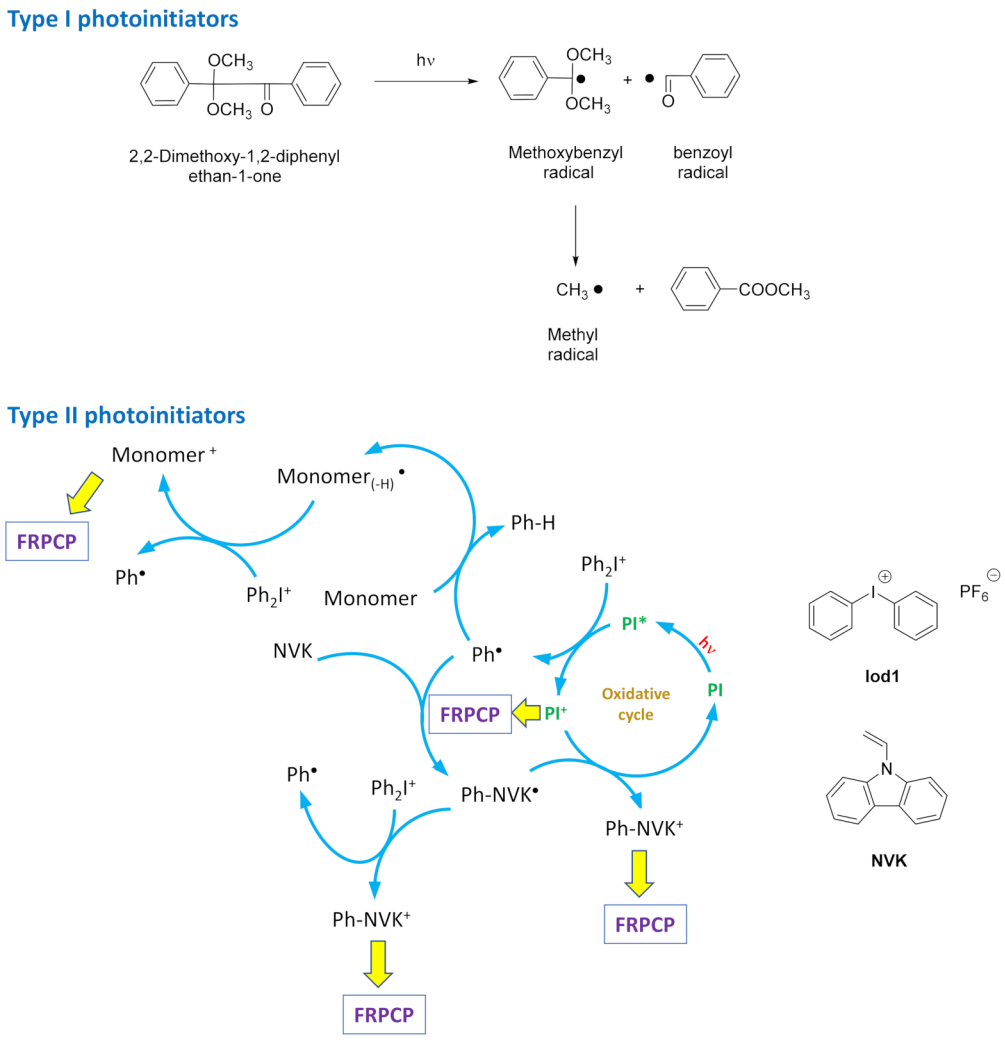

Figure 3. The two families of photoinitiators that have been developed in order to efficiently generate initiating radicals.

As shown in Figure 3, upon excitation of the photoinitiator with a light of an appropriate wavelength, a photoinduced electron transfer in the excited state can occur with the iodonium salt, generating phenyl radicals Ph$^{\bullet}$. These radicals can typically initiate the free-radical polymerization of acrylates. However, in these conditions, the consumption of the photosensitizer is irreversible, affecting the efficiency of the system. This drawback can be addressed by the addition of a third component—generally, a sacrificial amine that will be in charge of reducing the oxidized photosensitizer, and which can be introduced to the photocurable resin. If *N*-vinylcarbazole (NVK) is used, this carbazole can react with the phenyl radical Ph$^{\bullet}$, generating Ph–NVK$^{\bullet}$, which is a radical more reactive than the initial Ph$^{\bullet}$ [168]. By reacting with the oxidized photosensitizer and regenerating the photosensitizer at its initial redox state, Ph–NVK$^{\bullet}$ can be converted into a Ph–NVK^{+} cation, capable of initiating the cationic polymerization of epoxides by means of free-radical-promoted cationic polymerization (FRPCP). Therefore, using these three-component systems, the concomitant polymerization of acrylates and epoxides can be simultaneously obtained, enabling access to interpenetrated polymer networks (IPN) [169–172]. The photoinitiating systems are also catalytic if three-component systems are used, the regeneration of photoinitiators enabling the system to drastically reduce its content [173–175]. Considering that the photosensitizer is the key element of these two- and three-component photoinitiating systems, numerous structures have been examined. In this field, chalcones are dyes that can be naturally found in numerous vegetables and flowers [176–178]. Chalcones can also be easily obtained via a Claisen-Schmidt condensation. Considering their ease of synthesis, their strong absorption in the visible range, and their well-established biological activities, chalcones were investigated for applications ranging from medicine [179] to solar cell applications [180,181], organic light-emitting diodes [182], and organogels [183]. Among chalcones, *bis*-chalcones—which can be obtained via a Claisen-Schmidt condensation of aldehydes with cyclic aliphatic ketones in basic conditions—have been less studied in the literature than *mono*-chalcones [109,184]. Moreover, these structures remain of interest, especially for photopolymerization. Indeed, by increasing the molecular weight of photoinitiators, their migratability within the polymer network can be drastically reduced. These dyes also possess an extended conjugation compared to *mono*-chalcones; thus, these photosensitizers can transfer an electron towards an electron acceptor more easily in the excited state.

It should be noted that, in the past, chalcones have been investigated in photopolymerization, but as molecules capable of initiating [2 + 2] cycloaddition reactions [185]. However, in this case, chalcones were acting in the dual role of monomers and sensitizers, and not as sensitizers capable of initiating the polymerization of acrylates or epoxides. In this review, an overview of the different *bis*-chalcones reported to date as photoinitiators of polymerization is provided. Although the initial reports were devoted to investigating the photochemical mechanism of initiation rapidly, potential applications of these *bis*-chalcone-based photoinitiating systems have been examined. Comparisons with reference compounds will also be established in order to demonstrate the potential of these new structures for photoinitiation.

2. The Different Synthetic Routes to *bis*-Chalcones

Bis-chalcones have recently been studied as photoinitiators of polymerization, and three different strategies have been developed to provide access to these structures. Notably, chalcones can be easily obtained by means of a Claisen-Schmidt condensation between an aldehyde and an acetophenone, in accordance with the reaction depicted in Scheme 1 [186–195]. No major differences can be found from the synthetic viewpoint between *mono*- and *bis*-chalcones, except that two equivalents of aldehydes have to be used in the case of *bis*-chalcones, comprising a central cyclic ketone. In addition to this first strategy based on cyclic ketones, a second approach can consist of connecting two *mono*-chalcones together. In this aim, two connected aldehydes or two connected acetophenones can be used to form *bis*-chalcones.

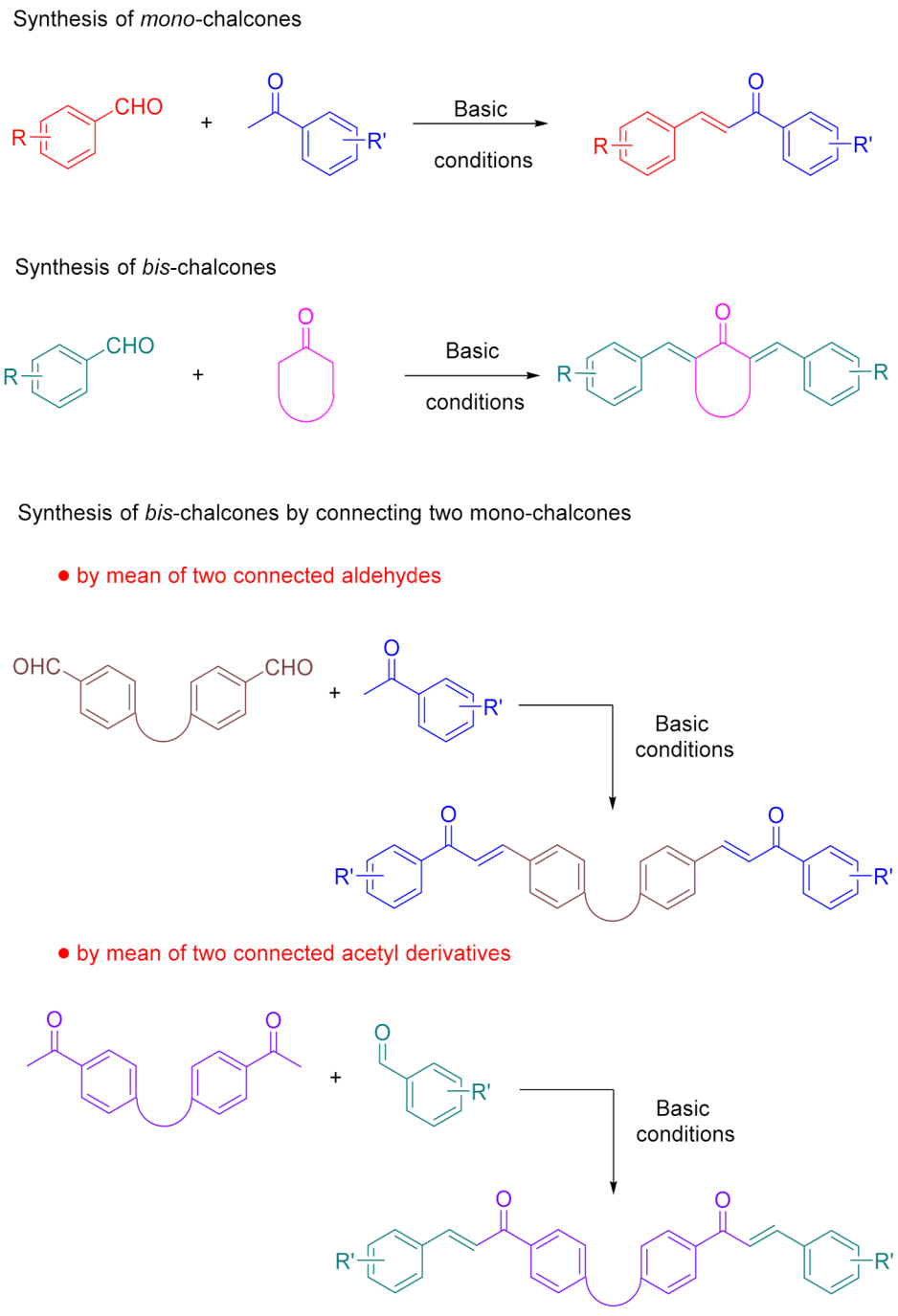

Scheme 1. Synthetic routes to *mono*- and *bis*-chalcones; and *bis*-chalcones obtained by connecting two *mono*-chalcones.

Based on the synthetic approach used to provide access to these structures, numerous modifications of the chalcone scaffold can be envisioned, such as a modification of the peripheral groups, the substitution pattern of the central cyclic aliphatic ketone, or the spacer introduced between the central core and the peripheral groups (see Figure 4). In the same spirit, *bis*-chalcones can be obtained via the condensation of acetophenones on *bis*-aldehydes. Aldehydes can also be condensed onto *bis*-acetophenones. Here, again, this strategy is highly versatile; since the spacer is used to connect the two chalcones, the substitution pattern of the chalcones can be easily tuned. Overall, the connection of two chalcones together enables a similar effect on the migratability of these macrophotoinitiators.

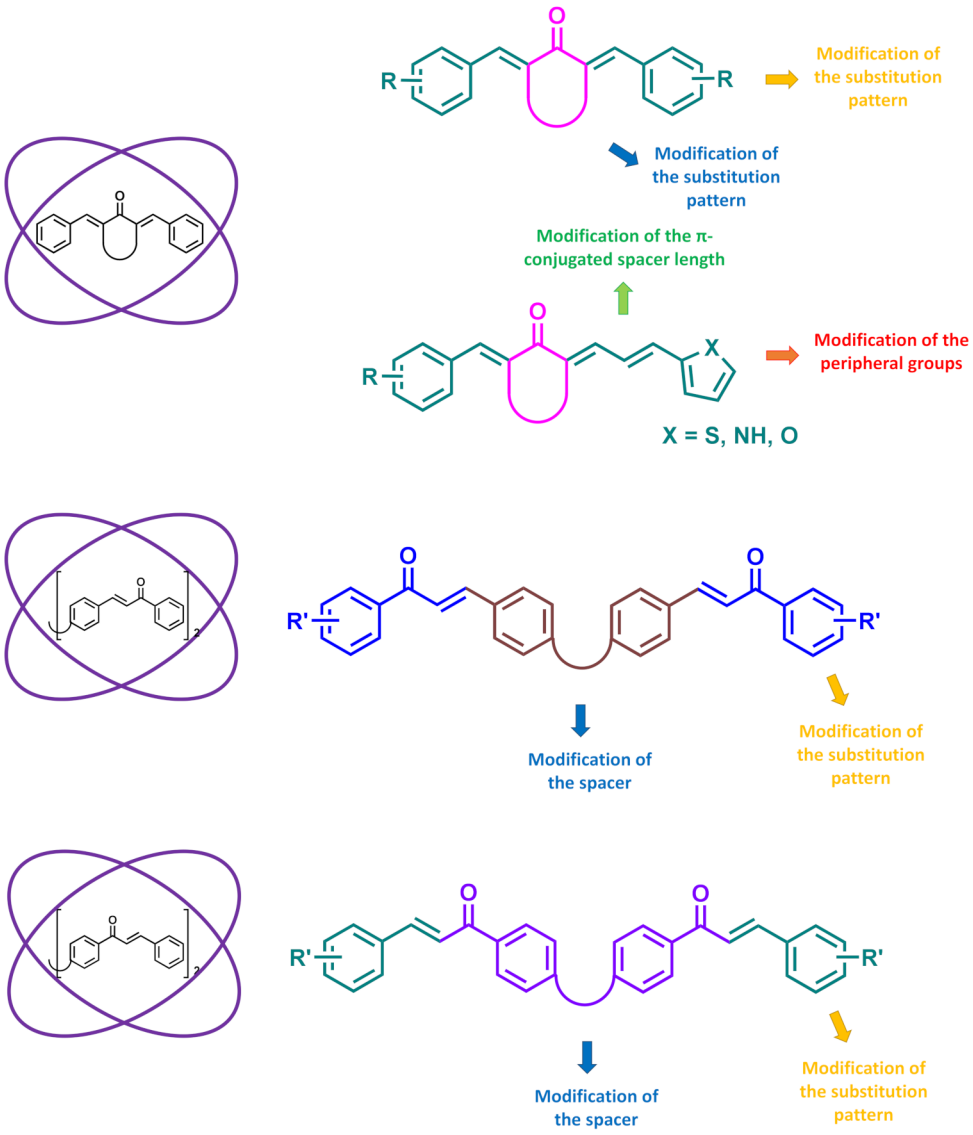

Figure 4. The different chemical modifications enabling the efficient tuning of the absorption spectra of *bis*-chalcones.

3. *Bis*-Chalcones as Photoinitiators

3.1. Bis-Chalcones Based on Cyclic Aliphatic Ketones

While *mono*-chalcones had been tested as early as 2014 as versatile photoinitiators for the free radical, cationic, and thiol-ene polymerizations of various monomers [196], the first report mentioning the use of *bis*-chalcones as photoinitiators of polymerization was by Lalevée et al. in 2020, wherein a series of six chalcones (C1–C6) was examined (see Figure 5) [197]. Interestingly, for this series of six *bis*-chalcones, two peripheral groups were selected—namely, pyrroles and thiophenes. Indeed, these two groups are well known to exhibit low oxidation potential [198–200]. Three different cyclic ketones were also used as the central cores—namely, *N*-ethylpiperidinone, *N*-benzylpiperidinone, and thiopyranone. From the absorption viewpoint, almost no difference was found between the absorption spectra of C1–C6 (see Figure 6 and Table 1). Indeed, absorption maxima ranging between 365 nm for C2 and 372 nm for C5 were determined using UV-visible absorption spectroscopy. However, C3 and C4 bearing *N*-ethylpiperidinone as the central core showed the highest molar extinction coefficients. At 405 nm, major differences could be found between the different dyes. Thus, if molar extinction coefficients lower than 100,000 $M^{-1}{\cdot}cm^{-1}$ were determined for C1 and C2 (9740 and 7980 $M^{-1}{\cdot}cm^{-1}$) at 405 nm,

molar extinction coefficients close to 120,000 $M^{-1} \cdot cm^{-1}$ could be determined for C3 and C5 at 405 nm. It should be noted that for all of these dyes, the molar extinction coefficients at 405 nm were greatly lowered compared to their absorption maxima located around 370 nm. Even if the absorption obtained at 405 nm only constitutes the edges of the absorption bands, this absorption and the molar extinction coefficients at these positions remain sufficient to initiate a polymerization process.

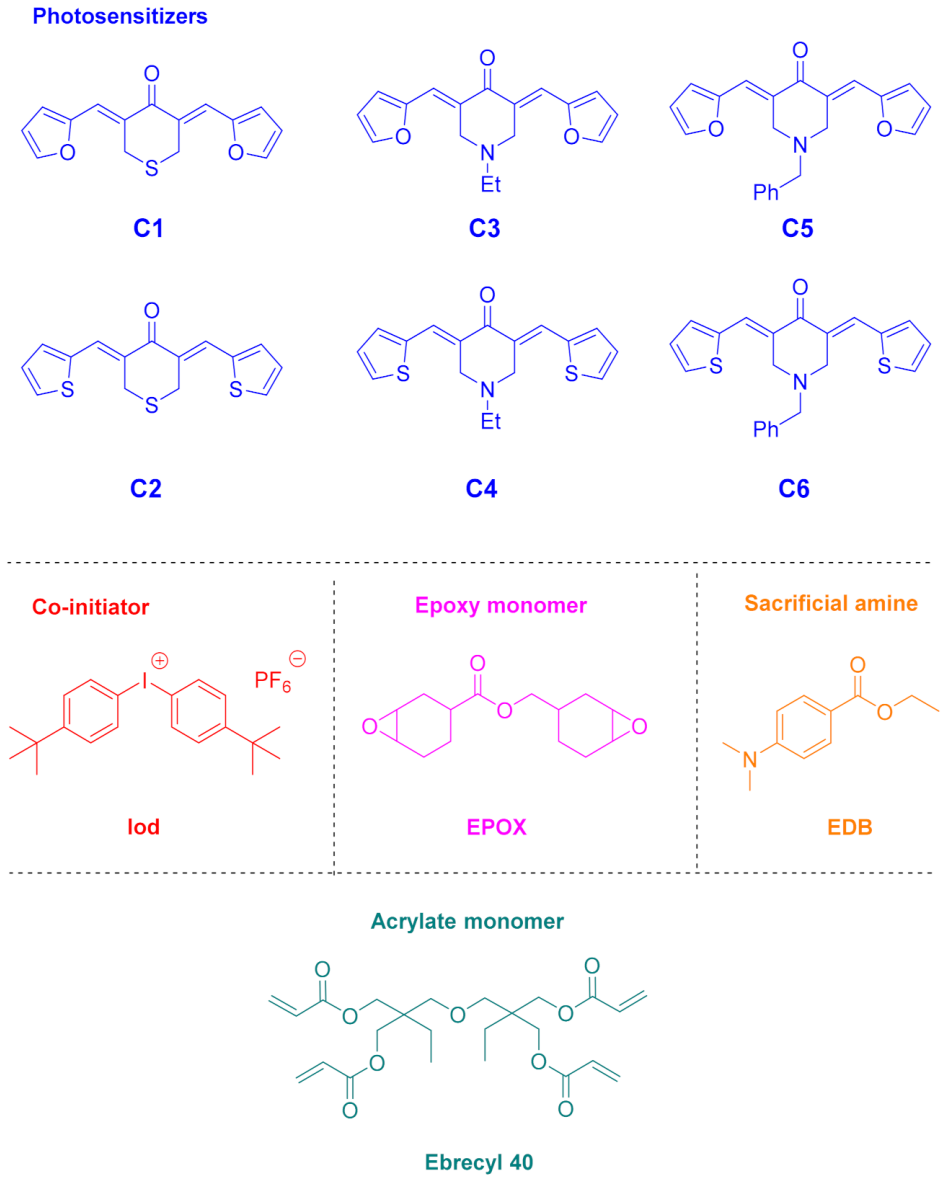

Figure 5. Chemical structures of C1–C6, the monomers, and the different additives.

Considering their absorptions at 405 nm, all of the dyes could be tested as photoinitiators at this wavelength. In order to get high monomer conversions, the different dyes were used in three-component systems, enabling *bis*-chalcones to be regenerated, and thus, to be introduced in catalytic amounts to the photoinitiating system. Using this strategy, an amount as low as 0.1 wt% could be used without adversely affecting the monomer conversion. While using the three-component chalcone/amine (EDB)/Iod (0.1%/2%/2%, *w*/*w*/*w*) photoinitiating systems (where EDB and Iod stand for ethyl dimethylaminobenzoate and 4,4′′-di-*tert*-butyldiphenyliodonium hexafluorophosphate, respectively), upon irradiation at 405 nm with an LED for 400 s, the best monomer conversions for thick films were obtained for C3 (94%) and C5 (90%), varying by the substitution pattern of the

central piperidinone core (ethyl or benzyl groups) (see Table 2). The decrease in monomer conversion determined for the C5-based photoinitiating system was attributed to the bulkiness of the benzyl group, providing a less densified polymer network. Conversely, all of the chalcones containing a sulfur atom in their structures furnished only low monomer conversions—lower than 30% after 400 s of irradiation. The lowest monomer conversions were obtained for C2 and C4 (24% conversion after 400 s of irradiation for both of the two dyes). Comparisons between the monomer conversions obtained with C3 (94%) and C4 (24%) revealed the detrimental effect of thiophene moiety on the photoinitiating ability of *bis*-chalcones, with the two dyes only differing by their peripheral groups.

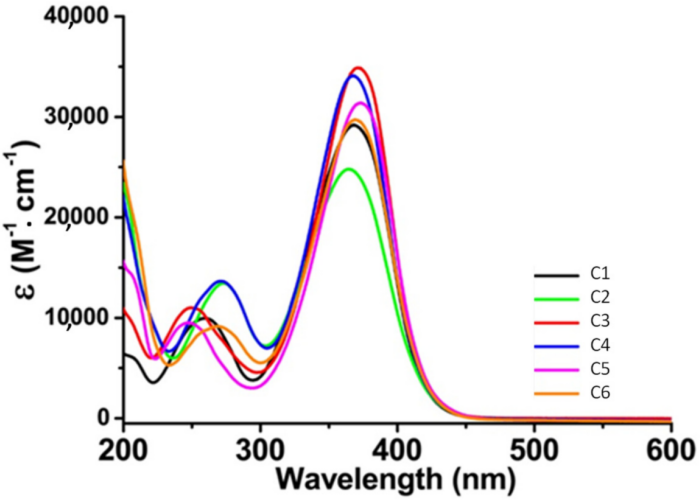

Figure 6. UV-visible absorption spectra of C1–C6 in acetonitrile. Reproduced from [197] with permission from The Royal Society of Chemistry.

Table 1. Light absorption properties of C1–C6 in acetonitrile.

Compounds	λ_{max} (nm)	ε_{max} ($M^{-1} \cdot cm^{-1}$)	$\varepsilon_{@405\ nm}$ ($M^{-1} \cdot cm^{-1}$)
C1	368	29,230	9740
C2	365	25,020	7980
C3	370	34,920	11,690
C4	368	34,200	10,130
C5	372	31,470	11,950
C6	370	29,750	10,280

Table 2. Final monomer conversions (FCs) for Ebecryl 40 in thick and thin films using chalcone/amine/Iod (0.1%/2%/2%, *w*/*w*/*w*), 405 nm LED, 400 s.

Compounds	C1	C2	C3	C4	C5	C6
FCs (thick films)	~30%	~24%	~94%	~24%	~90%	~25%
FCs (thin films)	~55%	~67%	~55%	~81%	~59%	~71%

An opposite trend was found for the polymerization of thin films. Indeed, in this last case, the C4-based photoinitiating system proved to be the most efficient one, enabling a monomer conversion rate of 81%. Although the C3-based three-component system could still initiate a polymerization process, the lowest monomer conversion rate in thin films was obtained with this system, peaking at 55%. This therefore clearly demonstrates the dramatic influence of the substitution pattern, as well as the choice of the central ketones, on the photoinitiating ability.

Considering that C3 could initiate polymerization in thick and in thin films, the polymerization mechanism was investigated using this dye. Photolysis experiments conducted in solution revealed C3 to efficiently interact with both the amine and the iodonium salt. Notably, a fast decrease in optical density was found upon irradiation at 405 nm for the two-component C3/amine and C3/Iod systems in acetonitrile. The ability of C3 to interact with reductive and oxidative processes was thus demonstrated (see Figure 7).

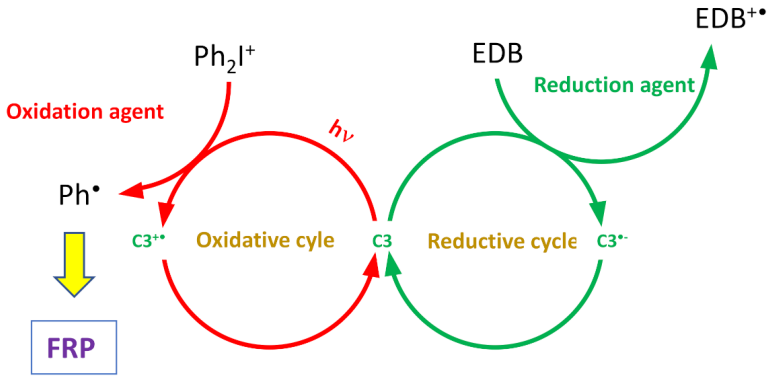

Figure 7. The dual role of C3 in three-component photoinitiating systems.

Interestingly, C3 could also initiate the cationic polymerization of (3,4-epoxycyclohexane) methyl 3,4-epoxycyclo-hexylcarboxylate (EPOX) using the two-component C3/Iod (0.1%/2%, *w*/*w*) system. After 400 s of irradiation at 405 nm, a monomer conversion of 50% could be obtained with an LED (I = 110 mW/cm^2). Finally, in light of the remarkable polymerization profiles obtained with C3, laser writing experiments were carried out with a laser (I = 100 mW/cm^2) emitting at 405 nm. As anticipated, 3D patterns with a high spatial resolution (100 µm) were obtained, and a 2-cm-length pattern could be polymerized within two minutes (see Figure 8). Conversely, in the same conditions, no 3D patterns could be obtained using the C4-based three-component photoinitiating system, consistent with the results obtained during the mechanistic investigations. In this last case, only a polymerization at the surface of the 3D patterns could be obtained.

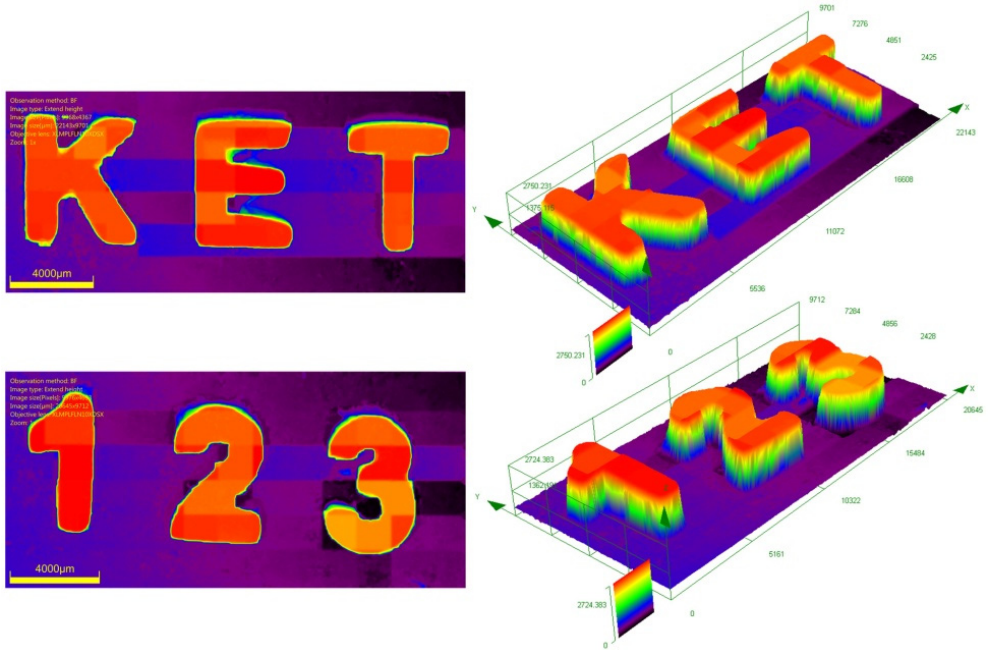

Figure 8. 3D patterns obtained during laser writing experiments using the C3-based three-component system. Reprinted from [197] Copyright (2020), with permission from Elsevier.

Following this initial work, another series of 13 *bis*-chalcones based on 6 different central cyclohexanones was examined in similar conditions to those used for the previous series (see Figure 9) [113]. From a synthetic viewpoint, all of these chalcones were obtained via a Claisen-Schmidt condensation, in a one-step reaction using aq. 40% KOH as the base, and the different dyes could be obtained with reaction yields ranging from 78% for C14 to 95% for C8. Ease of synthesis of such photoinitiators is of crucial interest from an industrial viewpoint, considering that most of the reagents (cyclohexanone derivatives, benzaldehyde derivatives, etc.) are cheap and commercially available. In this series, two groups of dyes could be identified.

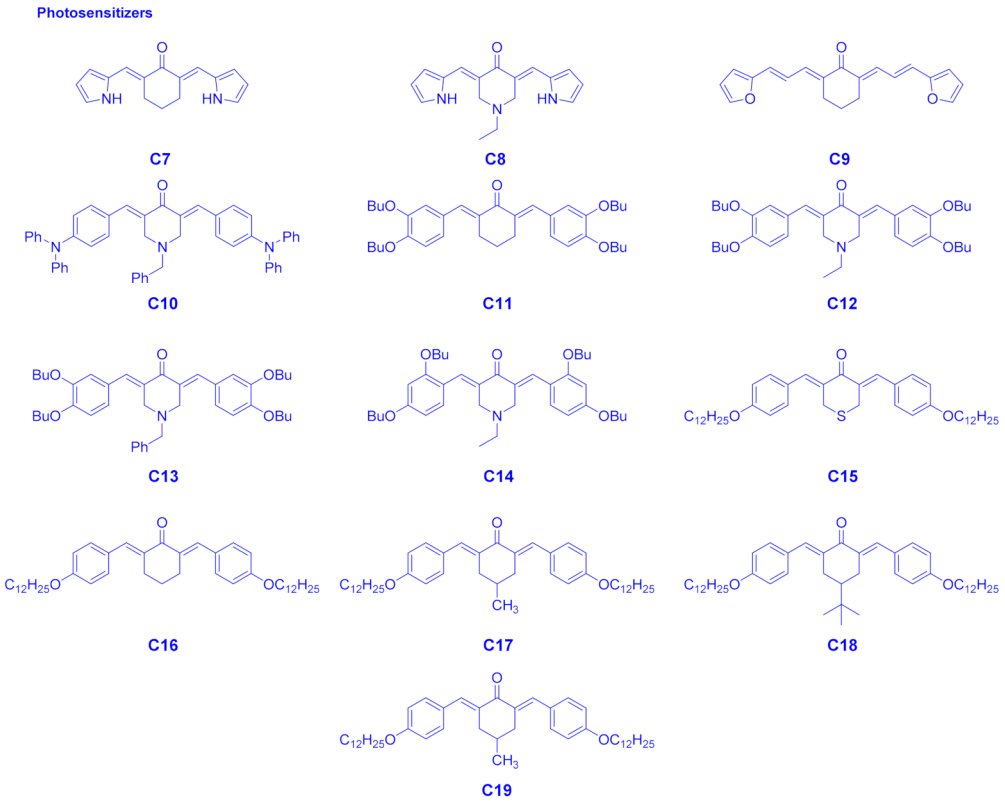

Figure 9. Chemical structures of C7–C19.

Thus, while C7–C10 absorbed in the visible range (405 nm for C8 and C9, 416 nm for C7, and 434 nm for C10), conversely, absorptions of C11–C19 remained centered in the UV range, with absorption maxima ranging from 350 nm for C15 and C16 to 375 nm for C12–C14 (see Table 3). However, a sufficient absorption at 405 nm could be determined for all dyes so that the polymerization experiments could be carried out.

Photopolymerization experiments conducted with the two-component chalcone/Iod (0.1%/2%, *w*/*w*) and chalcone/amine (0.1%/2%, *w*/*w*) revealed that the conversions of Ebecryl 40 with the different photoinitiating systems remained limited—lower than 55% and 40%, respectively. Similarly, control experiments performed with the different chalcones alone (0.1% *w*) revealed the monomer conversion to be low, peaking at 20%. Conversely, no polymerization could be initiated with EDB or Iod alone. While using the three-component chalcone/amine/Iod (0.1%/2%/2%, *w*/*w*/*w*) system, a significant enhancement of the monomer conversion could be evidenced, demonstrating the necessity of mixing the three components together in order to form an efficient photoinitiating system (see Figure 10).

Table 3. UV-visible absorption characteristics of C7–C19 in acetonitrile.

Compounds	λ_{max} (nm)	ε_{max} ($M^{-1}\cdot cm^{-1}$)	$\varepsilon_{405\ nm}$ ($M^{-1}\cdot cm^{-1}$)
C7	416	18,800	17,900
C8	405	36,200	36,200
C9	405	37,700	37,700
C10	434	30,800	23,000
C11	366	21,700	11,100
C12	375	25,200	15,500
C13	375	22,000	14,500
C14	375	23,400	15,800
C15	350	16,500	3100
C16	350	2800	900
C17	355	23,600	5300
C18	355	12,900	2700
C19	360	20,200	5700

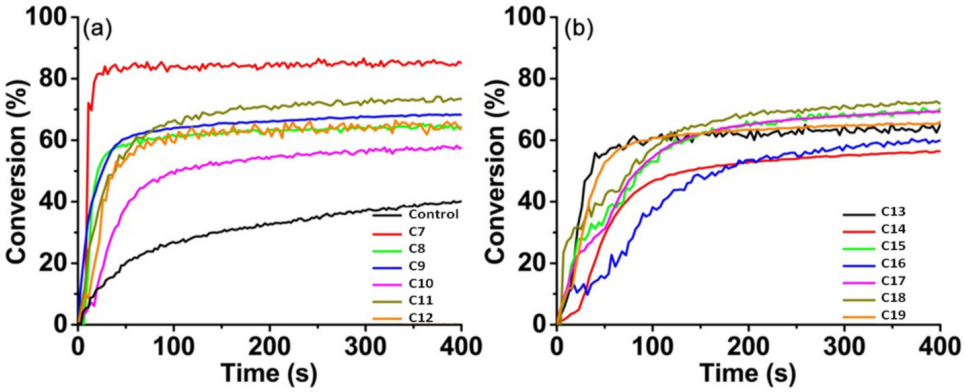

Figure 10. Polymerization profiles obtained using the three-component chalcone/amine/Iod (0.1%/2%/2%, *w*/*w*/*w*) system for C7–C12 (**a**) and C13–C19 (**b**); LED at 405 nm (110 mW/cm^2), in laminate. Control experiment: amine/Iod (2%/2%, *w*/*w*). Reprinted with permission from John Wiley & Sons, Inc. Copyright © [113].

Thus, monomer conversions ranging from 56% for C14 to 85% for C7 were determined after irradiation with an LED at 405 nm for 400 s in laminate (see Table 4). Among the different photoinitiating systems investigated, the three-component system based on C7 clearly outperformed the others, since an improvement of the monomer conversion of at least 10% could be obtained with this *bis*-chalcone. As shown in Figure 10, the different systems were nevertheless reactive, since the oxygen inhibition could be efficiently overcome. All of the polymerizations started immediately after the light was switched on, and this feature is characteristic of highly reactive photoinitiating systems [201–204]. While examining the influence of the peripheral groups, high monomer conversions could be obtained while using pyrrole as the peripheral group. Conversely, the lowest monomer conversions were obtained using the triphenylamine or 2,4-dibutoxyphenyl groups. In these two cases, monomer conversions peaking at 56% could be obtained using each of the two three-component systems. Interestingly, comparisons of the monomer conversions obtained between 2,4-dibutoxyphenyl- and 3,4-dibutoxyphenyl-substituted chalcones (C12 and C14) revealed an improvement of the conversion of nearly 10% with the 3,4-dibutoxyphenyl-substituted chalcone compared to the 2,4-dibutoxyphenyl-substituted chalcone, whereas the two chalcones exhibited similar absorption characteristics (absorption maxima, molar extinction coefficients). Therefore, the influence of the substitution pattern was clearly demonstrated. While examining the respective absorptions of the different chalcones at 405 nm, no direct correlations between absorption and monomer conversion could be established. Other parameters, such as the rate constants of interaction of the chalcones with the different additives, and the excited state lifetime, also have to be taken into account.

Notably, steady-state photolysis experiments revealed a consumption of 78% for C7 after 10 min of irradiation, while irradiating an acetonitrile solution containing C7 in combination with the iodonium salt. Conversely, under the same conditions, a consumption of only 32% was observed for C8, demonstrating that the photoinitiating ability of C7 was directly related to its higher photochemical reactivity with the iodonium salt, compared to C8–C19.

Table 4. Monomer conversions obtained with the three-component chalcone/amine/Iod (0.1%/2%/2%, *w*/*w*/*w*) system, LED at 405 nm (110 mW/cm^2), 400 s.

Photoinitiating Systems	FCs
Amine/Iod	
without chalcone	39%
C7	85%
C8	64%
C9	68%
C10	56%
C11	73%
C12	64%
C13	63%
C14	56%
C15	69%
C16	60%
C17	69%
C18	72%
C19	66%

The two-component C7/Iod (0.1%/2%, *w*/*w*) system also proved to be promising for initiating the cationic polymerization of epoxides. Thus, an EPOX conversion of 70% could be obtained with the C7/Iod (0.1%/2%, *w*/*w*) system upon irradiation at 405 nm with an LED, whereas the EPOX conversions were lower than 30% for the C8–C10-based photoinitiating systems (see Figure 11). The reactivity of the photoinitiating systems was highly dependent on the rate constants of interaction with the additives. Thus, while the photolysis experiments with the two-component C7/amine and C8/amine systems in acetonitrile revealed a consumption of the ketones of 11% and 12%, respectively, after 10 min of irradiation at 405 nm, higher declines were obtained with the C7/Iod and the C8/Iod systems, reaching 78% and 32%, respectively. Therefore, the higher photoreactivity of C7 compared to that of C8 is directly linked to the rate constant of interaction with the additives.

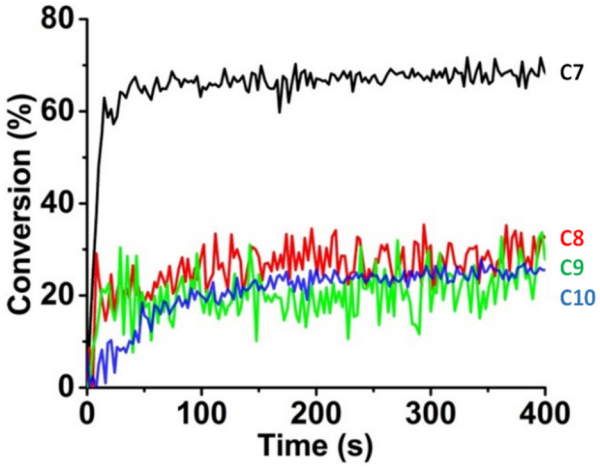

Figure 11. Polymerization profiles of EPOX obtained with two-component chalcone/Iod (0.1%/2%, *w*/*w*) systems upon irradiation at 405 nm with an LED. Reprinted with permission from John Wiley & Sons, Inc. Copyright © [113].

Similarly to that suggested for the first series of *bis*-chalcones, and on the basis of the photolysis experiments, an oxidation–reduction photochemical mechanism could be proposed to support the monomer conversions. These conclusions were confirmed by the fluorescence quenching experiments performed in acetonitrile. Determination of the electron transfer quantum yields revealed the C7/Iod system to exhibit a higher value (0.923) than that determined for the C8/Iod system (0.899).

Due to the high reactivity of the chalcone C7-based three-component system, the access to composites was thus examined. Indeed, the elaboration of composites remains a challenge with visible light photoinitiating systems, due to a limited light penetration and internal filter effects [205,206]. While introducing 20% weight of silica filler to Ebecryl 40, a severe limitation of the light penetration was demonstrated, as a light penetration of only 1.2 mm within the resin could be determined at 405 nm. By laser writing, 3D patterns exhibiting a remarkable spatial resolution could be obtained. An excellent dispersion of the fillers within the polymers could also be demonstrated by optical microscopy (see Figure 12).

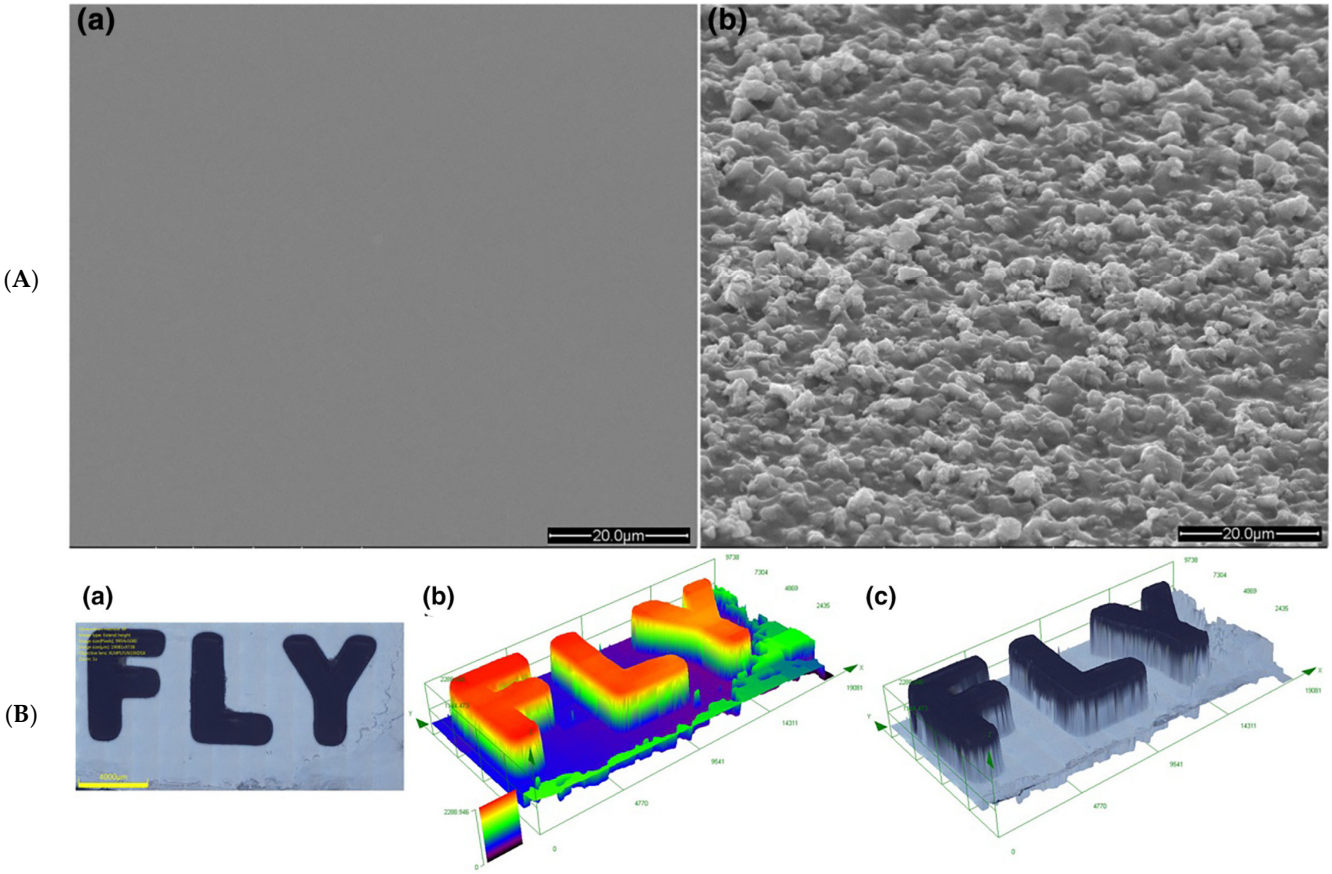

Figure 12. (**A**): SEM images of Ebecryl 40-based polymer, with (**a**) and without (**b**) silica fillers. (**B**): Images (**a**) (top view) and (**b**,**c**) (lateral view) obtained by numerical optical microscopy of 3D patterns obtained from laser writing experiments for resins containing 20% fillers, C7/amine/Iod (0.1%/2%/2%, *w*/*w*/*w*), 405 nm, 110 mW/cm^2. Reprinted with permission from John Wiley & Sons, Inc. Copyright © [113].

Peripheral groups of *bis*-chalcones can greatly influence the absorption spectra of dyes, and as such, a wide range of substituents has been examined over the years. Within a year, no less than 30 dyes differing by the peripheral groups have been proposed as photosensitizers, demonstrating the huge interest of photopolymerists in this family of compounds. Notably, the introduction of *para*-dimethylamino groups in C20–C25 enabled the development of dyes with absorption maxima ranging from 430 nm for C20, C21, and C23 to 436 nm for C24 and 440 nm for C25 (see Figures 13 and 14 and Table 5) [159]. Concerning the molar

extinction coefficients, the substitution pattern of the central cyclohexanone did not greatly influence the absorption properties, since molar extinction coefficients ranging between 40,000 $M^{-1} \cdot cm^{-1}$ for C23 and 49,900 $M^{-1} \cdot cm^{-1}$ for C22 could be determined in acetonitrile. A less intense absorption band was also detected in the UV range. A totally different situation was found for C26–C31. As shown in Figures 13 and 14, an intense absorption band was detected at 250 nm for all anthracene-based chalcones, whereas an intramolecular charge-transfer band could be detected for all dyes, with absorption maxima located in the UV range. Moreover, the ICT bands were broad, extending from 300 to 450 nm, such that a sufficient absorption could be found at 405 nm for performing photopolymerization experiments. However, a threefold reduction of the molar extinction coefficients could be determined at 405 nm for anthracene-based chalcones compared to dimethylaminophenyl-based chalcones. When tested as photosensitizers for three-component chalcone/amine/Iod (0.1%/2%/2%, *w*/*w*/*w*) systems, no direct correlation between the molar extinction coefficient at 405 nm and final monomer conversions could be established. Indeed, if the dimethylaminophenyl-based chalcones produced higher monomer conversions in thick films, the opposite situation was found in thin films, with the anthracene-based chalcones outperforming the dimethylaminophenyl-based chalcones (see Table 6 and Figure 15). However, shorter inhibition times and steeper slopes could be observed for the polymerization curves obtained with the dimethylaminophenyl-based chalcones (see Figure 15).

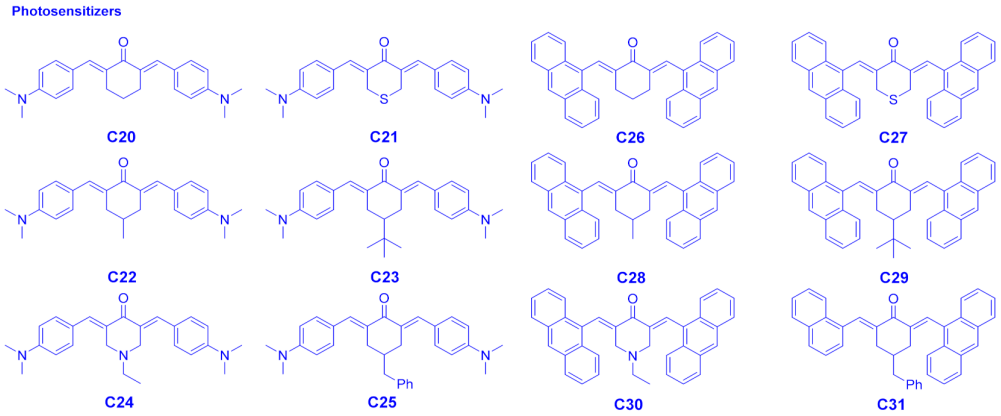

Figure 13. Chemical structures of C20–C31.

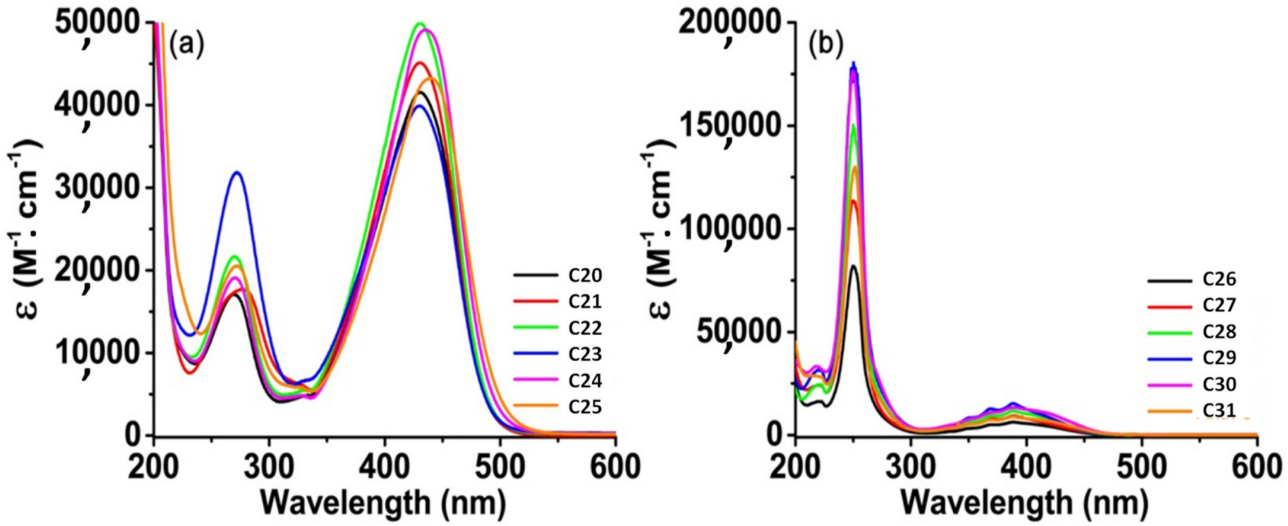

Figure 14. UV-visible absorption spectra of C20–C25 (**a**) and C26–C31 (**b**) in acetonitrile. Reproduced from [159] with permission from The Royal Society of Chemistry.

Table 5. Light absorption properties of the 12 different chalcones: absorption maxima wavelength (λ_{max}) as well as the molar extinction coefficients at λ_{max} (ε_{max}) and at 405 nm ($\varepsilon_{405\,nm}$), respectively.

Compounds	λ_{max} (nm)	ε_{max} (M^{-1} cm^{-1})	$\varepsilon_{405\,nm}$ (M^{-1} cm^{-1})
C20	430	41,600	31,900
C21	430	45,300	35,000
C22	431	49,900	38,400
C23	430	40,000	31,900
C24	436	49,200	34,200
C25	440	43,300	30,000
C26	250	81,800	5400
C27	250	113,300	7400
C28	250	149,600	9900
C29	250	178,400	11,500
C30	250	175,900	12,000
C31	250	129,500	7800

Table 6. Final monomer conversions obtained during the FRP of TA upon irradiation at 405 nm with an LED for 400 s using the three-component chalcone/amine/Iod (0.1%/2%/2%, *w*/*w*/*w*) systems.

FCs (in thick)	**C20**	**C21**	**C22**	**C23**	**C24**	**C25**
	~84%	~90%	~84%	~88%	~86%	~83%
	C26	**C27**	**C28**	**C29**	**C30**	**C31**
	~90%	~41%	~68%	~81%	~41%	~53%
FCs (in thin)	**C20**	**C21**	**C22**	**C23**	**C24**	**C25**
	~43%	~67%	~56%	~58%	~63%	~76%
	C26	**C27**	**C28**	**C29**	**C30**	**C31**
	~66%	~68%	~60%	~74%	~73%	~76%

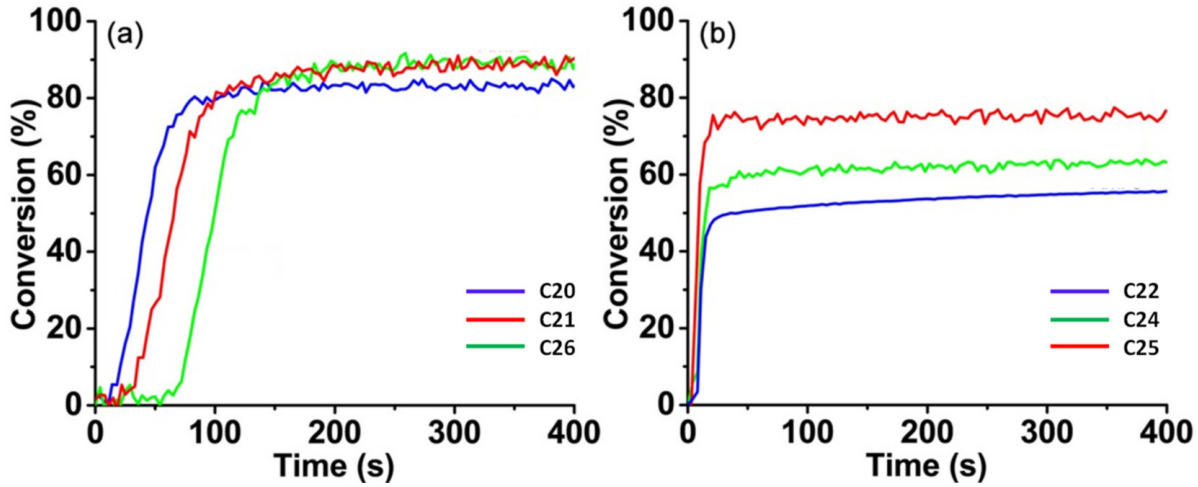

Figure 15. Photopolymerization profiles of TA, LED at 405 nm, using the three-component chalcone/amine/Iod (0.1%/2%/2%, *w*/*w*/*w*) photoinitiating systems: in thick films (1.4 mm) (**a**), and in thin films (25 μm) (**b**). Reproduced from [159] with permission from The Royal Society of Chemistry.

The extractability and migratability of photoinitiators is a major issue that can drastically affect future uses of polymers. In this context, in order to reduce the extractability of dyes, polymerizable groups can be introduced, as exemplified with C32–C36; for comparison, C14 [113], previously studied, was used as a non-crosslinkable chalcone (see Figure 16) [110].

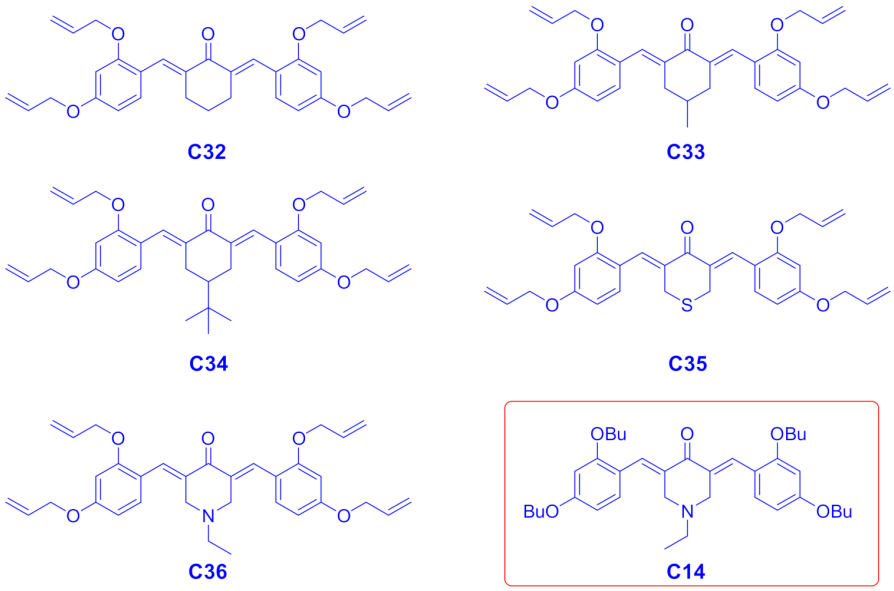

Figure 16. Chemical structures of crosslinkable chalcones C32–C36.

The comparison between the crosslinkable chalcone C36 and its non-crosslinkable version C14 revealed the remarkable migration stability of C36 compared to C14. Notably, for the polymers obtained with the three-component chalcone/amine/Iod (0.1%/2%/2%, *w*/*w*/*w*) photoinitiating systems, examination of the migratability of dyes in acetonitrile revealed that only 0.9% of the initial chalcone C36 could be extracted, as opposed to 8.3% for chalcone C14. Therefore, by introducing a crosslinkable group, a ninefold reduction of the migratability could be obtained.

Recently, a series of 12 *bis*-chalcones based on cyclopentanone was proposed, with similar peripheral groups to those used for the design of cyclohexanone-based chalcones (see Figure 17) [207].

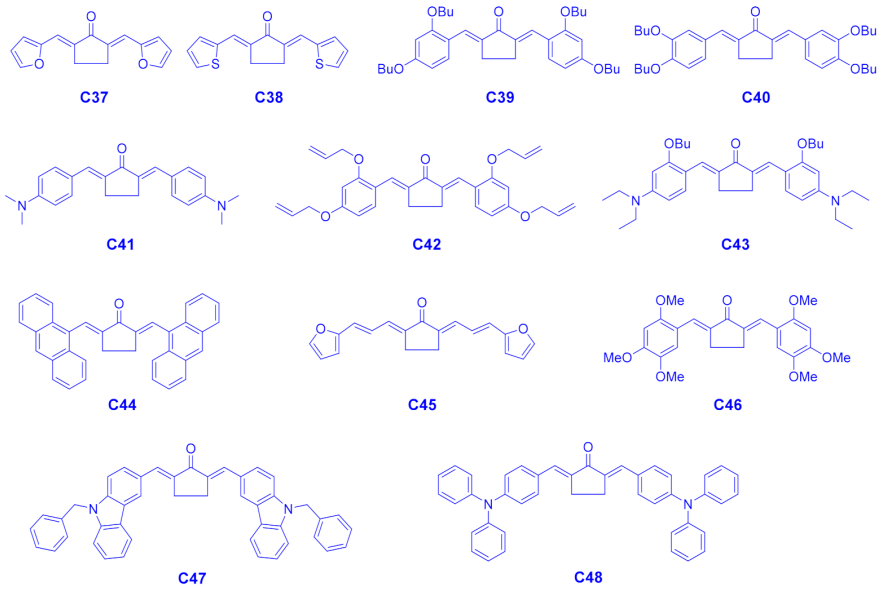

Figure 17. Chemical structures of C37–C48.

Interestingly, by replacing the cyclohexanone central part with a cyclopentanone moiety in these structures, a redshift of the ICT bands could be clearly demonstrated. Thus, if an absorption maximum located at 399 nm could be found for C40, its analogue based on cyclohexanone (i.e., C12, Figure 9) showed an absorption maximum at 375 nm,

blueshifted by ca. 25 nm (see Figure 18). The most redshifted absorption was determined for C43, with an absorption maximum peaking at 485 nm. To the best of our knowledge, C43 is the *bis*-chalcone exhibiting the most redshifted absorption ever used as photoinitiator of polymerization (485 nm, 65,670). The highest molar extinction coefficients could be determined for C41, C43, and C45, designed with the strongest electron-donating groups (see Table 7). Interestingly, in this work, the possibility of elaborating photocomposites via the in situ generation of silver nanoparticles was demonstrated. Indeed, by using the three-component chalcone/Iod/amine (0.1%/1.5%/1 wt%, *w*/*w*/*w*) system, phenyl radicals such as Ph•, but also Dye–H• and EDB•$_{(-H)}$, can react with the silver salt ($AgNO_3$), resulting in the reduction of the silver cation to Ag^0 and the formation of Ag nanoparticles via the aggregation of silver atoms, in accordance with the mechanism proposed in Figure 19.

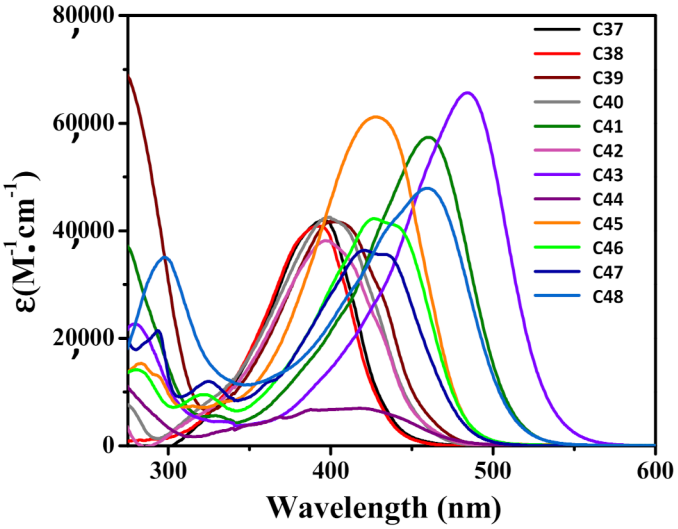

Figure 18. UV-visible absorption spectra of C37–C48 in acetonitrile. Reprinted with permission from John Wiley & Sons, Inc. Copyright© [207].

Table 7. Absorption characteristics of C37–C48 in acetonitrile.

Chalcone-Based Dyes	λ_{max} (nm)	ε_{max} ($M^{-1}\cdot cm^{-1}$)	$\varepsilon_{@405nm}$ ($M^{-1}\cdot cm^{-1}$)	$\varepsilon_{@470nm}$ ($M^{-1}\cdot cm^{-1}$)
C37	396	41,980	37,050	270
C38	392	40,840	33,590	110
C39	400 274	41,770 69,250	41,610	2,720
C40	399	42,500	41,580	1,280
C41	460 274	57,400 37,300	23,700	53,446
C42	397	38,150	36,700	1,710
C43	485 278	65,670 22,680	16,200	59,370
C44	418 268	6,970 12,890	6800	1,600
C45	428 283	61,130 15,340	50,310	16,540
C46	427 280	42,062 14,160	32,270	14,380
C47	421 236	36,350 46,810	30,560	10,160
C48	460 298	47,620 35,060	25,300	44,400

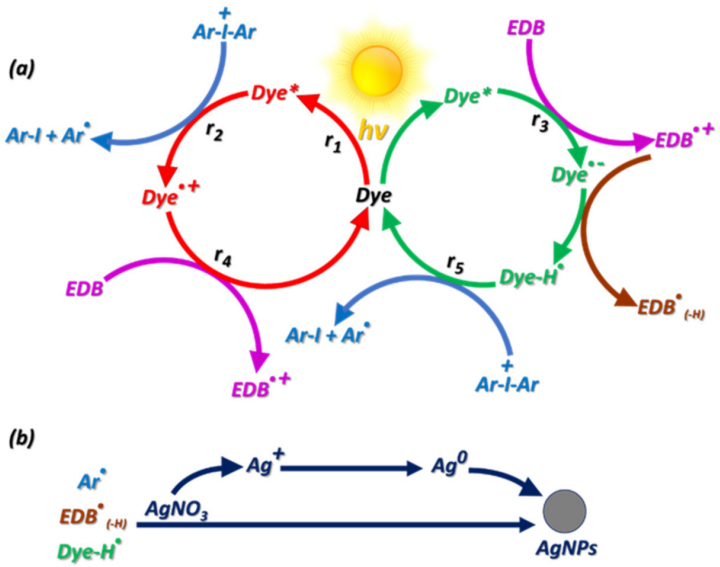

Figure 19. Mechanism of the photoinitiating systems enabling the formation of silver nanoparticles during the polymerization process. (**a**) catalytic cycle of polymerization (**b**) the mechanism of generation of Ag nanoparticles. Reprinted with permission from John Wiley & Sons, Inc. Copyright© [207].

In 2021, the previous trends established concerning the influence of the substitution pattern on the photoinitiating ability of *bis*-chalcones were confirmed by a new study [112]. In this work, four *bis*-chalcones (C49–C52) containing thiopyranone or benzylpiperidinone central cores were examined as photoinitiators for the free-radical polymerization of a polyethylene glycol (600) diacrylate (PEG-diacrylate) and the FRPCP of EPOX at 375 and 405 nm, respectively (see Figure 20).

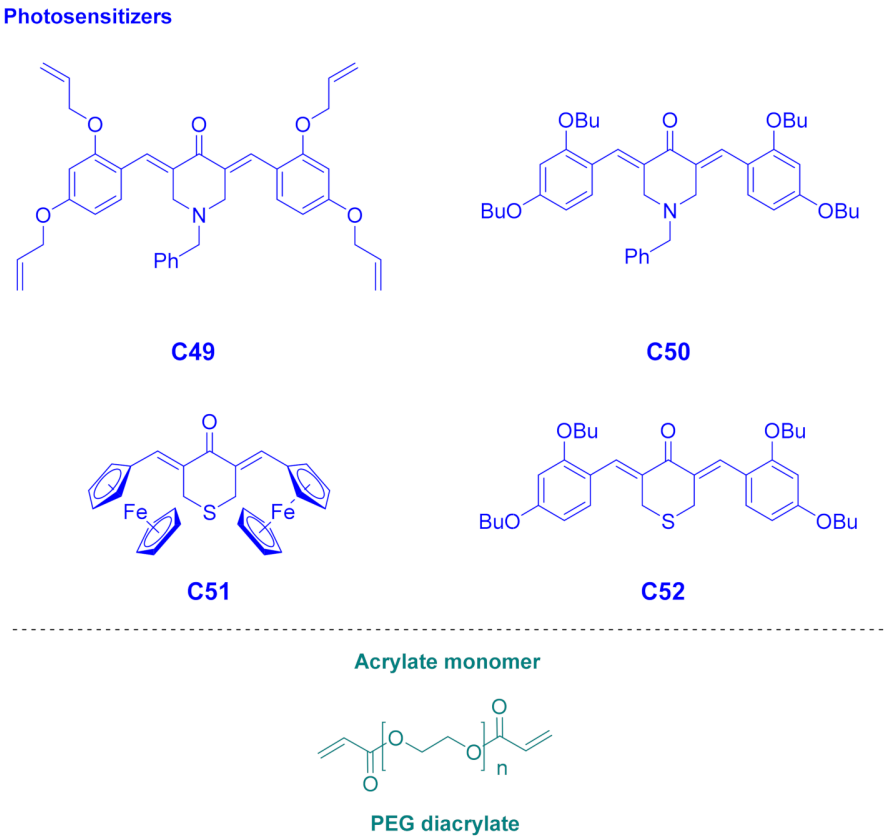

Figure 20. Chemical structures of C49–C52 and the acrylic monomer.

Interestingly, the presence of the ferrocene moiety in C51 enabled the drastic shift of the absorption maxima towards the visible range. Thus, absorption maxima located at 332 and 511 nm could be determined in acetonitrile for C51 (see Table 8). For the 3 other chalcones, UV-centered absorption maxima were found, peaking at 370, 380, and 369 nm for C49, C50, and C52, respectively. As anticipated, good monomer conversions could be obtained using the different three-component systems upon irradiation at 375 nm (40 mW/cm^2). As shown in Table 7, monomer conversions ranging between 89% for C50 and 60% for C51 could be determined while using the three-component photoinitiating chalcone/Iod/amine (1.5%/1.5%/1.5%, *w*/*w*/*w*) systems, and upon irradiation of the resin for 200 s. These monomer conversions were greatly higher than that obtained with the Iod/EDB combination (49%). At 405 nm, a reduction of the monomer conversion was logically observed, consistent with a reduction of the molar extinction coefficients at this wavelength. Thus, the highest conversion was obtained with C50 (79%), whereas the lowest ones were determined with C51 and C52 (42%). In fact, a clear correlation between molar extinction coefficients and final monomer conversions could be established at 405 nm. Interestingly, at the two irradiation wavelengths, ferrocene-based photoinitiating systems proved to be the worst candidates for photopolymerization, indicating that the introduction of ferrocene to chalcone was not convenient in developing highly efficient photoinitiators. These results were confirmed by other studies devoted to ferrocene-based chalcones used as photoinitiators of polymerization [208]. Conversely, ferrocene has historically been used to initiate the cationic polymerization of epoxides [120,209]. Furthermore, photopolymerization experiments performed at 375 nm revealed the C51-based three-component system C51/Iod/amine (1.5%/1.5%/1.5%, *w*/*w*/*w*) to give the worst EPOX conversion (66%). For the three other *bis*-chalcones, EPOX conversions higher than 70% could be obtained. Here, again, the best EPOX conversion was obtained with C52 (74%), whereas this dye exhibited the lowest molar extinction coefficient at 375 nm (4800 $M^{-1}\cdot cm^{-1}$). Therefore, the photoinitiating ability of C52 is related to its photochemical reactivity and the ease of forming *bis*-chalcone $^{+\bullet}$).

Table 8. UV-visible absorption characteristics of chalcones C49–C52 in acetonitrile. Acrylate and epoxide monomer conversions determined at 375 and 405 nm.

Chalcones	λ_{max} (nm)	ε_{max} ($M^{-1}\cdot cm^{-1}$)	$\varepsilon_{@375nm}$ ($M^{-1}\cdot cm^{-1}$)	$\varepsilon_{@405nm}$ ($M^{-1}\cdot cm^{-1}$)	PEG-Diacrylate Conversion		EPOX Conversion
					375 nm	405 nm	375 nm
C49	370	21,900	21,800	12,740	77	60	70
C50	380	28,200	28,000	19,730	89	79	72
C51	332 511	18,200 4940	5800	4420	60	42	66
C52	369	4980	4800	2550	82	42	74
blank 1	-	-	-	-	49	49	-
blank 2	-	-	-	-	-	-	45

Blank 1: Iod/amine (1.5%/1.5% *w*/*w*); blank 2: *bis*-chalcone/Iod/amine (1.5%/1.5%/1.5%, *w*/*w*/*w*).

It should be noted that the low photoinitiating ability of ferrocene-based dyes was confirmed with C54, which also provided lower final monomer conversions than C53 (86% vs. 95% during the FRP of PEG-diacrylate in thin films, 60% vs. 91% during the FRPCP of EPOX) (see Figure 21) [208].

In 2020, an elegant strategy was developed to create visible light and water-soluble photoinitiating systems from dyes absorbing in the UV range [210]. This result could be obtained by forming charge-transfer complexes between a *bis*-chalcone and a co-initiator—namely, triethanolamine (TEOA). Considering that TEOA is a water-soluble amine, a water-soluble charge-transfer complex could thus be obtained. Indeed, only few water-soluble photoinitiators are commercially available, as exemplified by 2-Hydroxy-4′-(2-hydroxyethoxy)-2-methylpropiophenone (Irgacure 2959). However, its water solubility is

limited, only reaching 0.5 wt%. Many approaches have been developed over the years to convert efficient photoinitiators into water-soluble structures. Moreover, such results can only be obtained after tedious and complex syntheses [211–215]. Conversely, the formation of charge-transfer complexes (CTCs) is an efficient strategy to easily produce numerous CTCs without requiring extensive synthetic works [216]. Over the years, numerous CTCs have been proposed as photoinitiating systems, such as 2-isopropylthioxanthonium phenacyl hexafluoroantimonate, which could form a CTC with *N*,*N*-dimethylaniline (DMA) [213]. Several CTCs have also been proposed by Lalevée et al., in order to develop dual photoassisted/thermal initiating systems [206,214,217–220]. In the present work, (2*E*,6*E*)-2,6-*bis*(furan-2-ylmethylidene)cyclohexan-1-one (C55) was used as an electron acceptor for TEOA (see Figure 22).

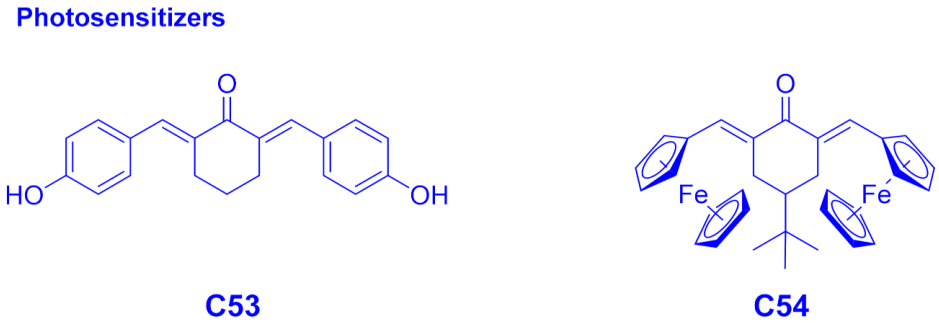

Figure 21. Chemical structures of C53 and C54.

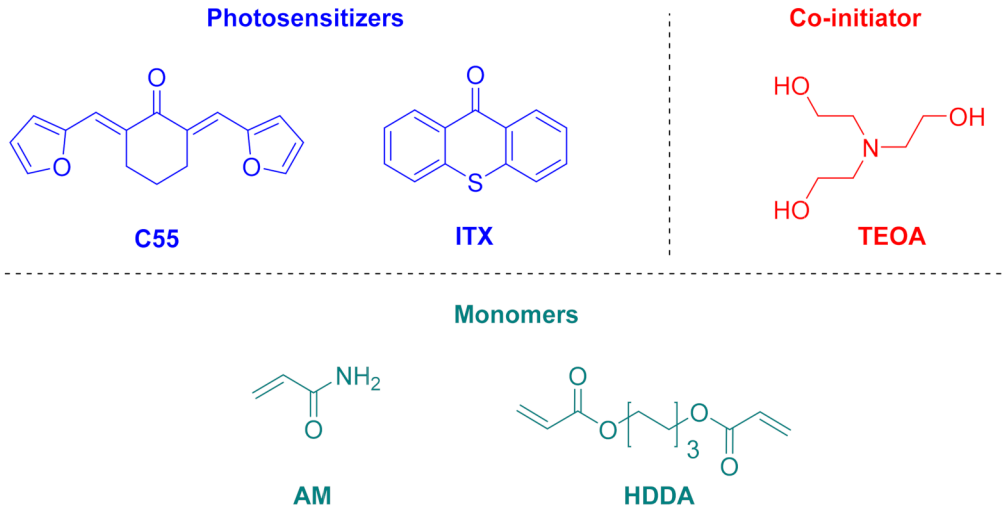

Figure 22. Chemical structures of C55, TEOA, and the monomer (AM).

By mixing the two compounds in acetonitrile, a redshift of the absorption could be clearly observed, from 373 nm for C55 to 400 nm for the [C55-TEOA] CTC (see Figure 23). A saturation concentration of 5 wt% in water was determined for the [C55-TEOA] CTC. While attempting to dissolve thioxanthone (ITX) in water by mixing ITX with TEOA, ITX was determined to separate out from TEOA, indicating that the formation of a CTC between the photoinitiator and the amine was required in order to maintain the water solubility of the photoinitiator. In this context, the [C55-TEOA] CTC was used as a photoinitiating system for the FRP of acrylamide (AM) in water upon irradiation at 405 nm with an LED ($I = 70\ mW/cm^2$), and a concentration varying from 0.5 wt% to 3 wt% was examined. Interestingly, upon increase of the concentration, an improvement of the monomer conversion was observed (see Figure 24). Moreover, 3 wt% was determined as the optimal concentration, with an optical shielding effect occurring at higher concentrations. Indeed, when the

concentration was too high, light penetration was adversely affected by an increase in the optical density, decreasing the monomer conversion.

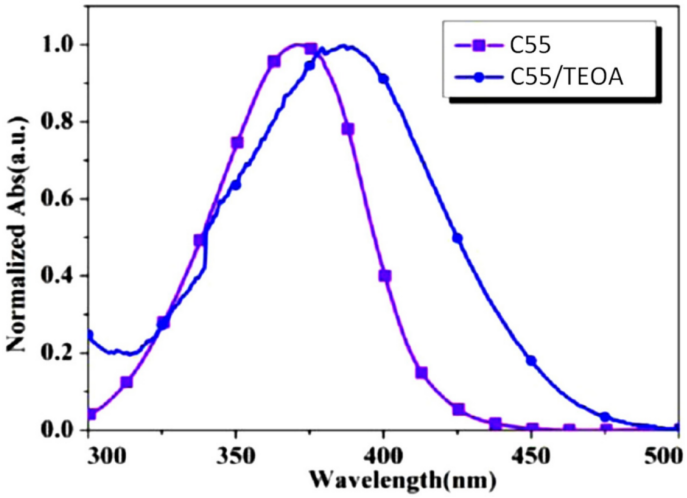

Figure 23. UV-visible absorption spectra of C55 and [C55-TEOA] CTC in acetonitrile. Reprinted from [210]; Copyright (2020), with permission from Elsevier.

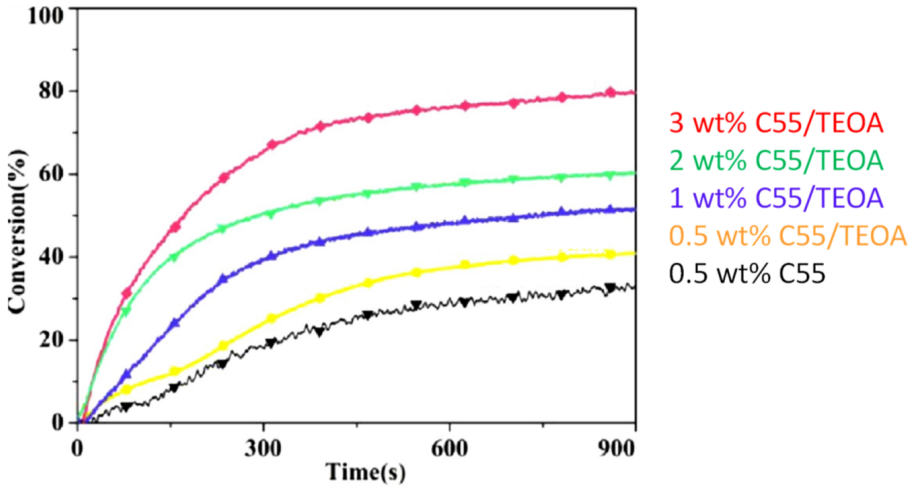

Figure 24. Polymerization profiles obtained upon irradiation at 405 nm (70 mW/cm^2) of an AM resin using the [C55-TEOA] CTC as the photoinitiating system. Reprinted from [210]; Copyright (2020), with permission from Elsevier.

C55 is an interesting photosensitizer, since this dye was also determined to interact strongly with certain monomers; a relevant example of this was demonstrated with PEG-diacrylate [156,158]. Comparison of the UV-visible absorption spectra of C55 in PEG diacrylate and hexamethylene diacrylate (HDDA) revealed the absorption spectrum in PEG-diacrylate to be drastically redshifted compared to that observed in HDDA (see Figure 25). Thus, at 405 nm, a molar extinction coefficient of 42,800 $M^{-1}{\cdot}cm^{-1}$ could be found for C55 in PEG-diacrylate, whereas a molar extinction coefficient of 35,900 $M^{-1}{\cdot}cm^{-1}$ was determined in PEGDA at 365 nm. Similarly, a redshift of the fluorescence was determined for C55 in PEG-diacrylate compared to that determined in HDDA, consistent with the trend observed for the absorption.

In fact, the formation of exciplexes with protonic monomers such as PEG-diacrylate was suggested to support the modification of the absorption spectra. Interestingly, the authors demonstrated PEG-diacrylate to act as an efficient co-initiator for C55. Thus, upon irradiation at 405 nm, a monomer conversion of 80% could be obtained within a few sec-

onds with the two-component C55/EDB (0.0625%/5% *w*/*w*) system in PEG-diacrylate, as opposed to 10% in HDDA. Replacement of EDB with PEG-diacrylate in the photoinitiating system enabled an increase in the HDDA conversion to 60% within a few seconds, upon irradiation at 405 nm of the two-component C55/PEG-diacrylate (0.0625%/5% *w*/*w*) system. The ability of PEG-diacrylate to act as a better co-initiator than the standard EDB was thus clearly demonstrated. Finally, comparison with a benchmark photoinitiator was established in order to demonstrate the potential of C55 as a photoinitiator (see Figure 26). Irrespective of the co-initiator (EDB or PEG-diacrylate), the two-component system based on C55 could clearly outperform that based on thioxanthone (ITX). Notably, in PEG-diacrylate, a 2.5-fold enhancement of the monomer conversion was observed with C55 compared to that obtained with ITX. The possibility of monitoring the polymerization process via photoluminescence measurements was also demonstrated by the same authors [157].

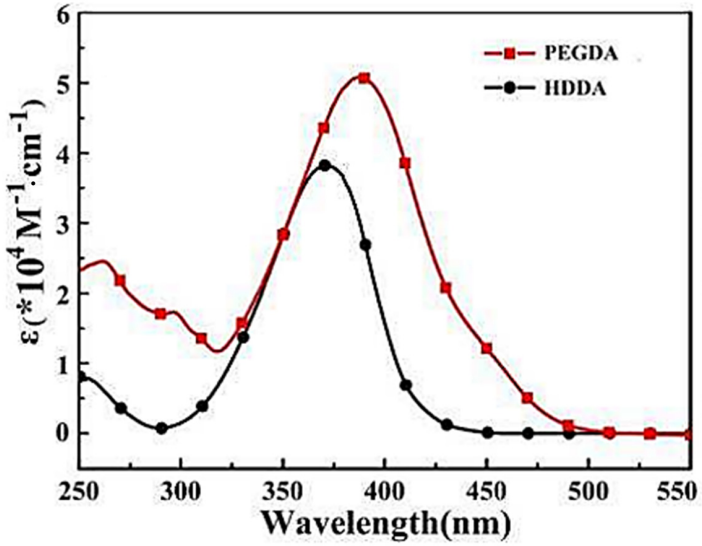

Figure 25. UV-visible absorption spectra of C55 in PEG-diacrylate and HDDA. Reprinted from [158]; Copyright (2019), with permission from Elsevier.

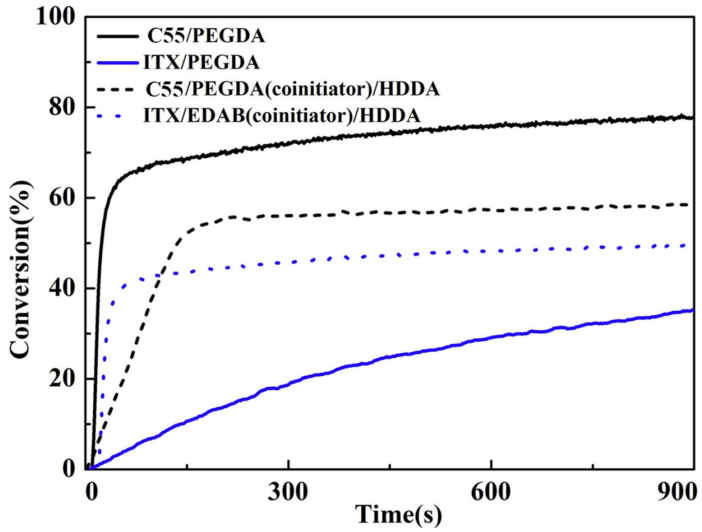

Figure 26. Comparisons of the polymerization profiles established for C55 and ITX used as a reference photoinitiator: C55 (0.0625% wt)/PEG-diacrylate, ITX (0.0625% wt)/PEG-diacrylate, C55 (0.0625% wt)/PEG-diacrylate (5% wt)/HDDA, ITX (0.0625% wt)/EDB (5% wt)/HDDA, LED at 405 nm, 70 mW/cm^2. Reprinted from [158]; Copyright (2019), with permission from Elsevier.

Finally, the mechanism depicted in Scheme 2 was proposed by the authors to support the formation of exciplexes and the ability of PEG-diacrylate to act as a co-initiator. Thus, by mixing C55 and PEG-diacrylate, hydrogen bonds can form between the oxygen atom of furan and the hydrogen atoms of the monomer. Upon photoexcitation, an electron transfer can occur between the electron-accepting C55 and the electron-rich monomer. Subsequently, by proton transfer between the radical cation of the monomer and the radical anion of C55, a radical can form on the monomer, initiating the polymerization process.

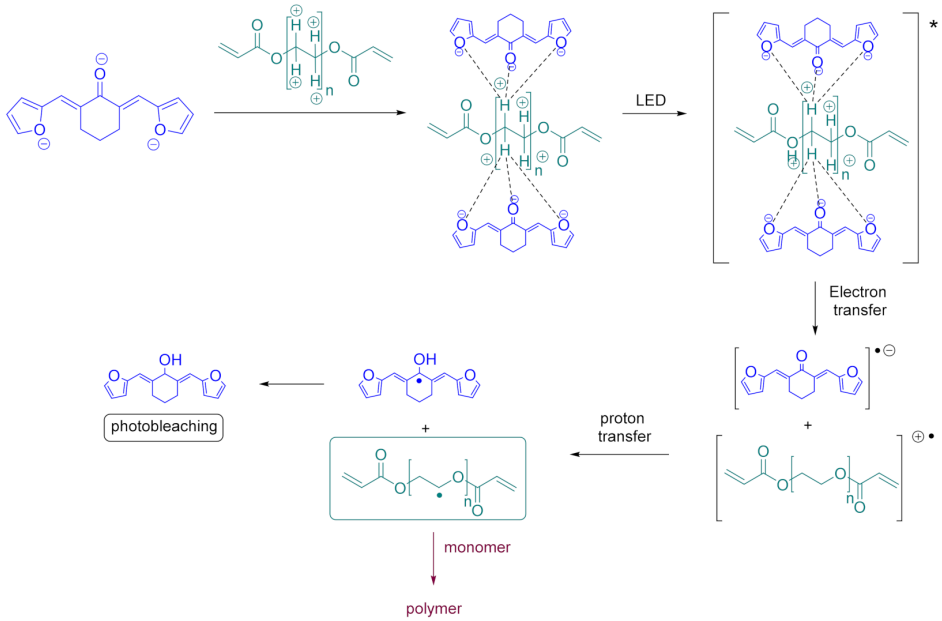

Scheme 2. Mechanism proposed to support the high photoinitiating ability of the C55/PEG-diacrylate combination. Reprinted from [158]; Copyright (2019), with permission from Elsevier.

Interestingly, efficient photobleaching of the resin was also demonstrated with C55, and this property is actively sought for visible light photoinitiating systems, these initiating systems being highly colored. Indeed, one major drawback of visible light photoinitiating systems is the color imposed by the photoinitiator, and an extensive body of work is notably devoted to developing photoinitiators capable of bleaching upon irradiation [221–223]. This ability was nevertheless demonstrated during the mechanistic investigations, as well as during the different 3D printing experiments, as shown in Figure 27. Indeed, after polymerization, a complete photobleaching could be obtained, and a colorless 3D structure could be prepared.

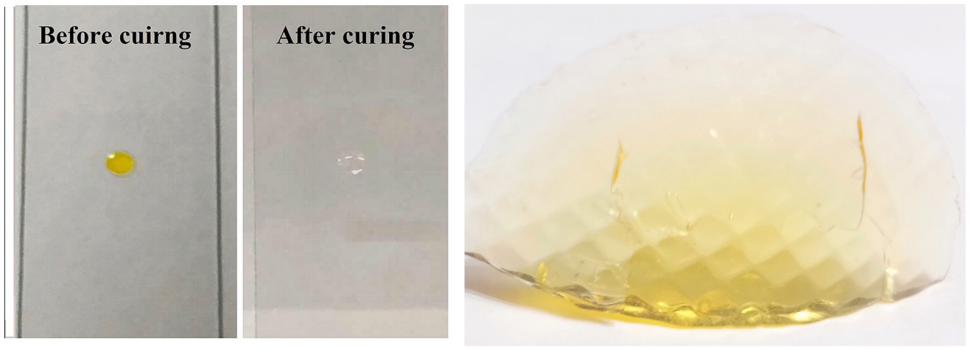

Figure 27. Left: photobleaching evidenced during the photopolymerization process; the resin before and after curing. **Right**: tridimensional structure obtained by 3D printing, exhibiting efficient photobleaching compared to the initial resin. Reprinted from [158]; Copyright (2019), with permission from Elsevier.

3.2. Bis-Chalcones Based on Two Connected Chalcones

Bis-chalcones based on cyclic aliphatic ketones have recently demonstrated their promising photoinitiating abilities, from the photopolymerization kinetic viewpoint, for final monomer conversions, but also in various practical applications. Furthermore, *mono*-chalcones are also efficient photoinitiators, and numerous such structures have been examined by several research groups. In an ever-ongoing effort to further improve monomer conversion, the covalent linkage of two chalcones has been examined as a potential strategy through which to optimize polymerization efficiency. Notably, structures resulting from this covalent linkage can exhibit a redshifted absorption compared to the chalcones considered separately, provided a π-conjugation exists between the two chalcones. Jointly, by increasing the molecular weight, extractability and migratability of the structures within the polymers can be efficiently avoided. In 2020, three structures (C57–C59) based on triphenylamine, connected by means of central *bis*-aldehydes and varying in their peripheral groups, were reported by Lalevée et al. (see Figure 28) [224]. For comparison, a *mono*-chalcone C56 was also prepared.

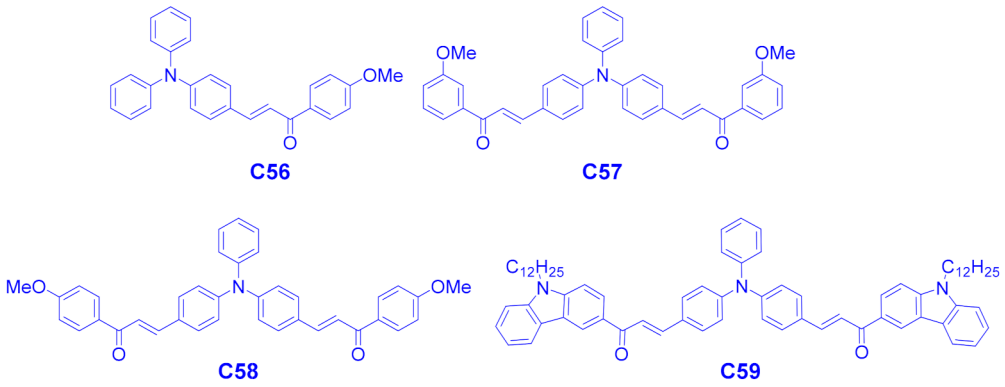

Figure 28. Chemical structures of *bis*-chalcones connected by mean of *bis*-aldehyde.

As shown in Table 9, use of 4,4′-(phenylazanediyl)dibenzaldehyde to form chalcones C57–C59 enabled the redshifting of their absorption maxima by ca. 30 nm compared to that of chalcone C56. Indeed, if an absorption maximum at 405 nm was found for C56, the absorption maxima shifted to 430 nm for chalcones C57–C59. Interestingly, no significant influence of the peripheral groups was determined, since the replacement of a methoxyphenyl-based acetophenone by a carbazole-based acetophenone did not modify the position of the absorption maximum. Considering their absorption, the 4 chalcones were appropriate for photopolymerization experiments carried out at 405 nm, since molar extinction coefficients higher than 6000 $M^{-1} \cdot cm^{-1}$ were determined at 405 nm. Conversely, the connection of the two chalcones by means of a π-conjugated system resulted in a significant decrease of the molar extinction coefficient. If a molar extinction coefficient of 18,740 $M^{-1} \cdot cm^{-1}$ was measured in acetonitrile for C56, a twofold reduction of the molar extinction coefficient was determined for its analogue C58 (8540 $M^{-1} \cdot cm^{-1}$).

Table 9. Light absorption properties of chalcones C56–C59 in acetonitrile.

Compounds	λ_{max} (nm)	ε_{max} ($M^{-1} \cdot cm^{-1}$)	$\varepsilon_{@405nm}$ ($M^{-1} \cdot cm^{-1}$)
C56	405	18,740	18,740
C57	430	7990	6760
C58	428	8540	7200
C59	430	10,500	9020

Four different photoinitiating systems were used to initiate the FRP of PEG diacrylate in both thick and thin films—namely, the three-component chalcone/Iod/EDB (1.5%/1.5%/1.5%, *w*/*w*/*w*) photoinitiating system, the two-component chalcone/Iod

(1.5%/1.5%, *w*/*w*) and chalcone/EDB (1.5%/1.5%, *w*/*w*) photoinitiating systems, and the chalcones alone (1.5% *w*). While no polymerization could be initiated with the chalcones alone, only thin films could be polymerized with the two-component chalcone/EDB (1.5%/1.5%, *w*/*w*) photoinitiating systems. Conversely, for the two-component chalcone/Iod (1.5%/1.5%, *w*/*w*) and the three-component chalcone/Iod/EDB (1.5%/1.5%/1.5%, *w*/*w*/*w*) photoinitiating systems, photopolymerization could be efficiently initiated both in thin and thick films (see Table 10), providing higher final monomer conversions than the two-component chalcone/EDB (1.5%/1.5%, *w*/*w*) photoinitiating systems. Interestingly, higher final monomer conversions were obtained with the two-component chalcone/Iod (1.5%/1.5%, *w*/*w*) than with the three-component chalcone/Iod/EDB (1.5%/1.5%/1.5%, *w*/*w*/*w*) photoinitiating systems, assigned to a competition with the electron-donating groups in chalcones and EDB. As a result of this, all three-component photoinitiating systems based on chalcones C57–C59 furnished lower final monomer conversions than the control experiment (blank) composed only of Iod/EDB (1.5%/1.5%, *w*/*w*). Conversely, the three-component PI systems based on chalcone C56 furnished a final monomer conversion on par with that of the blank control. Therefore, it could be concluded that EDB was inhibiting the generation of free radicals—the opposite situation to that which is commonly found for the three-component PIs. Interestingly, the three-component chalcone C56/Iod/EDB (1.5%/1.5%/1.5%, *w*/*w*/*w*) photoinitiating system and the two-component C56/Iod (1.5%/1.5%, *w*/*w*) photoinitiating system could initiate polymerization in thick films under daylight, evidencing the high reactivity of these two PIs. A polymerization ending within a few minutes could be demonstrated.

Table 10. Final monomer conversions obtained during the FRP of PEG diacrylate at 405 nm after 200 s of irradiation for thin films, and 600 s of irradiation for thick films, using the two-component chalcone/Iod (1.5%/1.5%, *w*/*w*) system and the three-component chalcone/Iod/EDB (1.5%/1.5%/1.5%, *w*/*w*/*w*) photoinitiating system.

Chalcones	Chalcone/Iod/EDB		Chalcone/Iod	
	Thin Films	Thick Molds	Thin Films	Thick Molds
C56	71%	92%	82%	94%
C57	58%	53%	77%	52%
C58	85%	17%	93%	21%
C59	85%	77%	93%	92%
blank	50%	93%		

Considering the high reactivity of PIs based on chalcones C56 and C59, PEG-based polymers were prepared, and due to the good affinity of PEG polymers for water, swelling experiments were carried out with polymers prepared with C56 and C59. After printing an "H" pattern in laser writing experiments using the two-component chalcone/Iod (1.5%/1.5%, *w*/*w*) system, the swelling of the PEG-based polymers was examined by immersing the polymers in water. Interestingly, a good correlation between polymerization rates and swelling ratios was determined. Thus, the highest swelling ratio was obtained for the polymers prepared with chalcone C59 (80%), due to a lower polymerization rate obtained with this chalcone compared to that obtained with chalcone C56 (92% vs. 94% monomer conversions in thick film). After swelling, a 2–3-fold enhancement of the volumes of the different 3D patterns could be determined (see Figure 29).

In 2021, a series of *bis*-chalcones (C60–C65) connected by mean of *bis*-acetyl spacers was examined as photoinitiators of polymerization (See Figure 30) [112]. However, compared to the previous strategy—which enabled the generation of photoinitiators absorbing until 430 nm—in the present case, the absorption of pyridine-based chalcones and biphenyl-based chalcones was UV-centered, the main absorption band being located at 350–370 nm (see Table 11). As a result of this, low molar extinction coefficients were determined at 405 nm, i.e., the emission wavelength of the light source commonly used in 3D printers. As anticipated, due to better adequation of their absorption maxima with the emission spectrum of the LED at

375 nm, higher final monomer conversions were obtained at 375 nm than at 405 nm, consistent with their molar extinction coefficients at the two wavelengths (see Table 11).

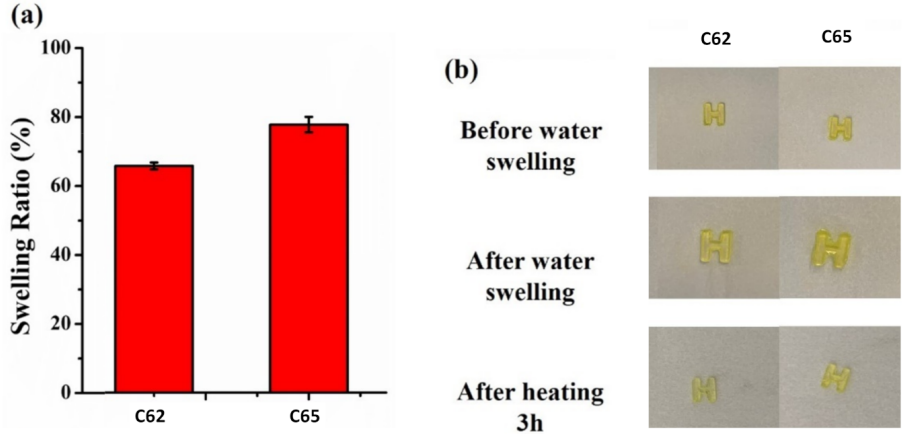

Figure 29. (**a**) Swelling ratios determined for PEG-based polymers prepared with C62 and C65; (**b**) pictures of the polymer 24 h after swelling and after 3 h of heating for dehydration. Reprinted from [224]; Copyright (2020), with permission from Elsevier.

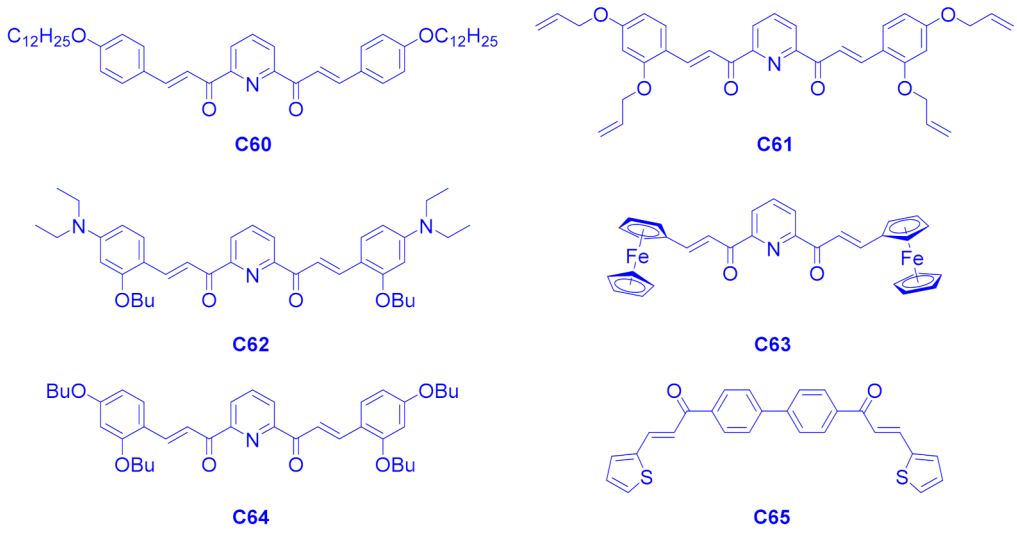

Figure 30. Chemical structures of *bis*-chalcones connected by mean of *bis*-acetyl spacers.

Table 11. UV-visible absorption properties of *bis*-chalcones C60–C65 in acetonitrile.

Chalcones	λ_{max} (nm)	ε_{max} ($M^{-1} \cdot cm^{-1}$)	$\varepsilon_{@405nm}$ ($M^{-1} \cdot cm^{-1}$)	$\varepsilon_{@375nm}$ ($M^{-1} \cdot cm^{-1}$)
C60	347	23,100	6800	16,500
C61	364	22,700	10,070	21,500
C62	430	38,900	26,420	8500
C63	330	19,800	2960	4000
C64	370	24,600	13,670	24,000
C65	350	49,300	2220	24,500

As shown in Table 12, higher monomer conversions than that obtained with the blank control could only be obtained based on Iod/EDB (1.5%/1.5%, *w*/*w*), demonstrating the crucial role of *bis*-chalcones in photoinitiation. At 375 nm, the highest monomer conversion was obtained for *bis*-chalcone C61 (95%) during the FRP of PEG diacrylate. Conversely, at 405 nm, the best conversion was determined for *bis*-chalcone C62 (95%).

No direct relation between molar extinction coefficients and final monomer conversions at the two wavelengths could be established. Similarly, significant differences between *bis*-chalcones C61 and C64 could be determined in terms of final monomer conversions, even though the two chalcones only differ by alkyl chains. Here, again, the lowest monomer conversions were obtained at 375 and 405 nm for the ferrocene-based *bis*-chalcone, once again evidencing the detrimental effect of this substituent.

Table 12. Final monomer conversions determined during the FRP of PEG diacrylate using the 5%/1.5%/1.5%, *w*/*w*/*w*) photoinitiating systems shown in Table 1, at 375 and 405 nm.

LED@375 nm							
Chalcones	C60	C61	C62	C63	C64	C65	Blank
FCs	86	95	80	64	89	82	49
LED@405 nm							
Chalcones	C60	C61	C62	C63	C64	C65	Blank
FCs	62	83	95	53	91	62	49

Finally, swelling experiments were carried out with *bis*-chalcones C60 and C64. Indeed, swelling experiments carried out with PEG polymers prepared with *bis*-chalcones C60 and C64 showed good swelling ratios, ranging from 60% for C60 to 70% for C64. Increases in volume as high as 160% and 143% could be determined for polymers prepared with *bis*-chalcones C60 and C65, respectively. Upon heating at 50 °C for 1 h, hydrated polymers could return to their initial appearances and volumes, demonstrating the reversibility of this hydration process. Consequently, the two photoinitiating systems were determined to be ideal candidates for 4D printing experiments. Indeed, hydration and dehydration of the hydrophilic PEG polymer can be advantageously used for shape modification. More precisely, 4D printing consists of elaborating an object of precise thickness and shape that can be modified subsequent to the polymerization process by means of an external stimulus such as heat [225–228], light [229], water [230–232], or other stimuli. Thus, after printing a cross with a high spatial resolution via 3D printing using the three-component chalcone/Iod/EDB (1.5%/1.5%/1.5%, *w*/*w*/*w*) photoinitiating systems based on chalcones C60 and C64, swelling and thermally induced dehydration resulted in significant modification of the shapes of the crosses. Thus, upon hydration, a complete deformation of the cross could be demonstrated. Upon heating at 50 °C, dehydration of the hydrophilic polymer could be obtained, enabling the cross to return to its initial shape (see Figure 31).

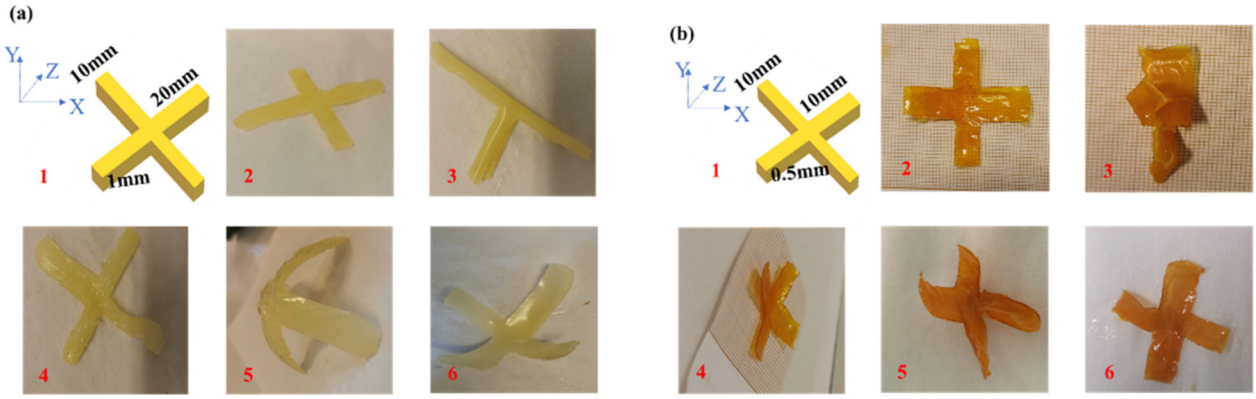

Figure 31. Swelling and dehydration cycles realized on 3D-printed crosses obtained using the three-component C60/Iod/EDB (1.5%/1.5%/1.5%, *w*/*w*/*w*) photoinitiating system (**a**) and using the three-component C64/Iod/EDB (1.5%/1.5%/1.5%, *w*/*w*/*w*) photoinitiating system (**b**). 1: structure of the cross; 2: cross after photopolymerization; 3: cross after one minute in water; 4: cross after 100 s of dehydration at 100 °C; 5: cross after 10 min of dehydration at 100 °C; 6: cross after 10 min at room temperature. Reproduced from [112] with permission from The Royal Society of Chemistry.

Here, again, the polymerization rate could govern the level of deformation. Indeed, due to a higher polymerization rate with *bis*-chalcone C60 compared to that obtained with *bis*-chalcone C64, less important deformations could be obtained for the PEG polymers. Conversely, for PEG polymers printed with *bis*-chalcone C64, the cross could not even be recognized after 1 min of swelling in water (see Figure 31b3). After 100 s of dehydration at 100 °C, recovery of its initial shape could be obtained.

4. Conclusions

In this review, an overview of the different *bis*-chalcones reported to date as photoinitiators of polymerization has been reported. Interest in *bis*-chalcones is a recent development, following the first report mentioning the use of *bis*-chalcones as photoinitiators by Wang et al., in 2019. Since then, numerous achievements have been attained. Notably, a water-soluble photoinitiator could be obtained with C55. Photobleaching properties could also be demonstrated with this dye. Moreover, Lalevée et al. examined various *bis*-chalcones varying by their central cores and the substitution patterns of their peripheral groups. Several trends could be established. Thus, the presence of ferrocene or thiophene as peripheral groups in *bis*-chalcones was determined to drastically decrease monomer conversion. A similar effect could be evidenced with thiopyranone as the central core. Interestingly, the influence of the substitution pattern of the central cyclic aliphatic ketone was determined to only marginally impact the absorption spectra (see Figure 32), and only chalcones absorbing between 350 and 550 nm could be obtained. Among the most interesting findings, the high reactivity of chalcones enabled their access to photocomposites, and the polymerization of resins containing 20% glass fillers could be successfully achieved. Considering that the absorption of chalcones remains limited in the 350–550 nm range, future works will consist of developing *bis*-chalcones capable of absorption at longer wavelengths, enabling a higher light penetration within the photocurable resins, and easier access to photocomposites.

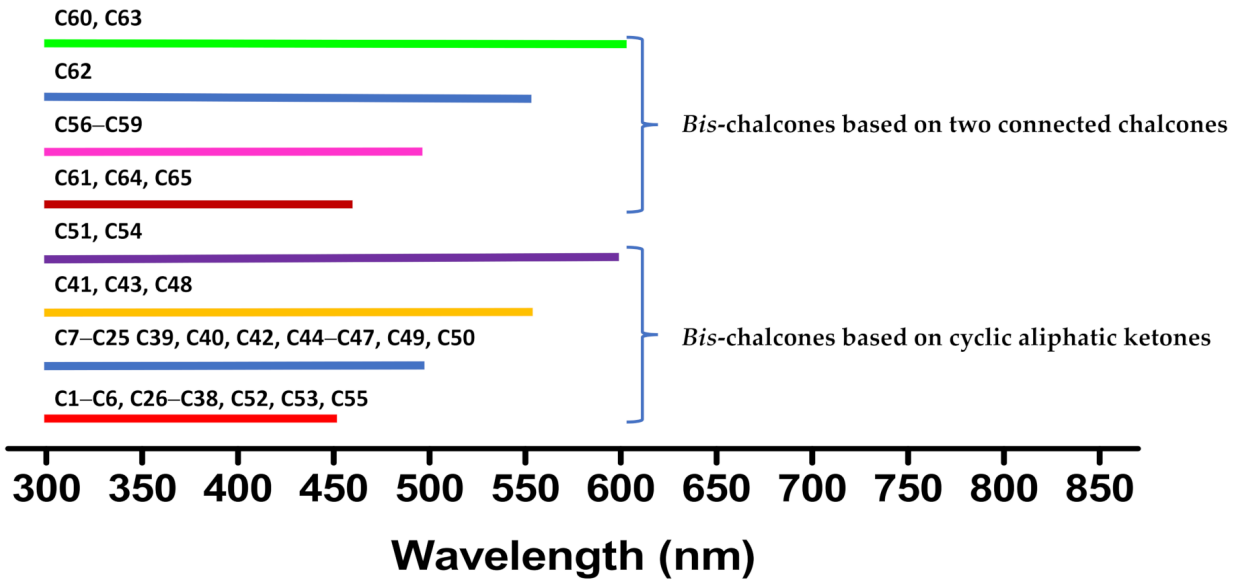

Figure 32. Absorption range of the *bis*-chalcones depicted in this review.

Author Contributions: Conceptualization, N.G. and F.D.; validation, N.G. and F.D.; resources, F.D.; writing—original draft preparation, N.G. and F.D.; writing—review and editing, N.G. and F.D.; visualization, N.G. and F.D.; supervision, N.G. and F.D.; project administration, F.D.; funding acquisition, F.D. All authors have read and agreed to the published version of the manuscript.

Funding: This research was funded by the Agence Nationale de la Recherche (ANR) through the PhD grant of Nicolas Giacoletto (ANR-19-CE07-0042, NO PEROX project).

Acknowledgments: Aix Marseille University and the Centre National de la Recherche Scientifique (CNRS) are acknowledged for financial support.

Conflicts of Interest: The authors declare no conflict of interest.

References

1. Hatton, F.L. Recent advances in RAFT polymerization of monomers derived from renewable resources. *Polym. Chem.* **2020**, *11*, 220–229. [CrossRef]
2. Nothling, M.D.; Fu, Q.; Reyhani, A.; Allison-Logan, S.; Jung, K.; Zhu, J.; Kamigaito, M.; Boyer, C.; Qiao, G.G. Progress and Perspectives Beyond Traditional RAFT Polymerization. *Adv. Sci.* **2020**, *7*, 2001656. [CrossRef]
3. Tian, X.; Ding, J.; Zhang, B.; Qiu, F.; Zhuang, X.; Chen, Y. Recent Advances in RAFT Polymerization: Novel Initiation Mechanisms and Optoelectronic Applications. *Polymers* **2018**, *10*, 318. [CrossRef] [PubMed]
4. Audran, G.; Bagryanskaya, E.G.; Marque, S.R.A.; Postnikov, P. New Variants of Nitroxide Mediated Polymerization. *Polymers* **2020**, *12*, 1481. [CrossRef] [PubMed]
5. Sciannamea, V.; Jérôme, R.; Detrembleur, C. In-Situ Nitroxide-Mediated Radical Polymerization (NMP) Processes: Their Understanding and Optimization. *Chem. Rev.* **2008**, *108*, 1104–1126. [CrossRef]
6. Audran, G.; Bagryanskaya, E.; Edeleva, M.; Marque, S.R.A.; Parkhomenko, D.; Tretyakov, E.; Zhivetyeva, S. Coordination-Initiated Nitroxide-Mediated Polymerization (CI-NMP). *Aust. J. Chem.* **2018**, *71*, 334–340. [CrossRef]
7. Shao, J.; Huang, Y.; Fan, Q. Visible light initiating systems for photopolymerization: Status, development and challenges. *Polym. Chem.* **2014**, *5*, 4195–4210. [CrossRef]
8. Park, H.K.; Shin, M.; Kim, B.; Park, J.W.; Lee, H. A visible light-curable yet visible wavelength-transparent resin for stereolithography 3D printing. *NPG Asia Mater.* **2018**, *10*, 82–89. [CrossRef]
9. Yoshino, F.; Yoshida, A. Effects of blue-light irradiation during dental treatment. *Jpn. Dent. Sci. Rev.* **2018**, *54*, 160–168. [CrossRef]
10. Garra, P.; Dietlin, C.; Morlet-Savary, F.; Dumur, F.; Gigmes, D.; Fouassier, J.-P.; Lalevée, J. Redox two-component initiated free radical and cationic polymerizations: Concepts, reactions and applications. *Prog. Polym. Sci.* **2019**, *94*, 33–56. [CrossRef]
11. Fouassier, J.-P.; Allonas, X.; Burget, D. Photopolymerization reactions under visible lights: Principle, mechanisms and examples of applications. *Prog. Org. Coat.* **2003**, *47*, 16–36. [CrossRef]
12. Fiedor, P.; Pilch, M.; Szymaszek, P.; Chachaj-Brekiesz, A.; Galek, M.; Orty, J. Photochemical Study of a New Bimolecular Photoinitiating System for Vat Photopolymerization 3D Printing Techniques under Visible Light. *Catalysts* **2020**, *10*, 284. [CrossRef]
13. Mendes-Felipe, C.; Oliveira, J.; Etxebarria, I.; Vilas-Vilela, J.L.; Lanceros-Mendez, S. State-of-the-art and future challenges of UV curable polymer-based smart materials for printing technologies. *Adv. Mater. Technol.* **2019**, *4*, 1800618. [CrossRef]
14. Shukla, V.; Bajpai, M.; Singh, D.K.; Singh, M.; Shukla, R. Review of basic chemistry of UV-curing technology. *Pigm. Resin Technol.* **2004**, *33*, 272–279. [CrossRef]
15. Chen, M.; Zhong, M.; Johnson, J.A. Light-controlled radical polymerization: Mechanisms, methods, and applications. *Chem. Rev.* **2016**, *116*, 10167–10211. [CrossRef] [PubMed]
16. Crivello, J.V.; Reichmanis, E. Photopolymer materials and processes for advanced technologies. *Chem. Mater.* **2014**, *26*, 533–548. [CrossRef]
17. Bonardi, A.-H.; Dumur, F.; Grant, T.M.; Noirbent, G.; Gigmes, D.; Lessard, B.H.; Fouassier, J.-P.; Lalevée, J. High performance near infrared (NIR) photoinitiating systems operating under low light intensity and in presence of oxygen. *Macromolecules* **2018**, *51*, 1314–1324. [CrossRef]
18. Scanone, A.C.; Casado, U.; Schroeder, W.F.; Hoppe, C.E. Visible-light photopolymerization of epoxy-terminated poly(dimethylsiloxane) blends: Influence of the cycloaliphatic monomer content on the curing behavior and network properties. *Eur. Polym. J.* **2020**, *134*, 109841. [CrossRef]
19. Garra, P.; Bonardi, A.-H.; Baralle, A.; Al Mousawi, A.; Bonardi, F.; Dietlin, C.; Morlet-Savary, F.; Fouassier, J.-P.; Lalevée, J. Monitoring photopolymerization reactions through thermal imaging: A unique tool for the real-time follow-up of thick samples, 3D Printing, and composites. *J. Polym. Sci. A Polym. Chem.* **2018**, *56*, 889–899. [CrossRef]
20. Sun, K.; Pigot, C.; Chen, H.; Nechab, M.; Gigmes, D.; Morlet-Savary, F.; Graff, B.; Liu, S.; Xiao, P.; Dumur, F.; et al. Free radical photopolymerization and 3D printing using newly developed dyes: Indane-1,3-dione and 1H-cyclopentanaphthalene-1,3-dione derivatives as photoinitiators in three-component systems. *Catalysts* **2020**, *10*, 463. [CrossRef]
21. Lalevée, J.; Mokbel, H.; Fouassier, J.-P. Recent developments of versatile photoinitiating systems for cationic ring opening polymerization operating at any wavelengths and under low light intensity sources. *Molecules* **2015**, *20*, 7201–7221. [CrossRef] [PubMed]
22. Tehfe, M.-A.; Louradour, F.; Lalevée, J.; Fouassier, J.-P. Photopolymerization reactions: On the way to a green and sustainable chemistry. *Appl. Sci.* **2013**, *3*, 490–514. [CrossRef]
23. Podsiadły, R.; Maruszewska, A.; Michalski, R.; Marcinek, A.; Kolinska, J. Naphthoylene benzimidazolone dyes as electron transfer photosensitizers for iodonium salt induced cationic photopolymerizations. *Dyes Pigm.* **2012**, *95*, 252–259. [CrossRef]
24. Zhang, Z.; Corrigan, N.; Bagheri, A.; Jin, J.; Boyer, C. A versatile 3D and 4D printing system through photocontrolled raft polymerization. *Angew. Chem.* **2019**, *131*, 18122–18131. [CrossRef]
25. Bagheri, A.; Engel, K.A.; Anderson Bainbridge, C.W.; Xu, J.; Boyer, C.; Jin, J. 3D printing of polymeric materials based on photo-RAFT polymerization. *Polym. Chem.* **2020**, *11*, 641–647. [CrossRef]

26. Bagheri, A.; Jin, J. Photopolymerization in 3D Printing. *ACS Appl. Polym. Mater.* **2019**, *1*, 593–611. [CrossRef]
27. Aduba, D.C., Jr.; Margaretta, E.D.; Marnot, A.E.C.; Heifferon, K.V.; Surbey, W.R.; Chartrain, N.A.; Whittington, A.R.; Long, T.E.; Williams, C.B. Vat photopolymerization 3D printing of acid-cleavable PEG-methacrylate networks for biomaterial applications. *Mater. Today Commun.* **2019**, *19*, 204–211. [CrossRef]
28. Lin, J.-T.; Cheng, D.-C.; Chen, K.-T.; Liu, H.-W. Dual-wavelength (UV and blue) controlled photopolymerization confinement for 3D-printing: Modeling and analysis of measurements. *Polymers* **2019**, *11*, 1819. [CrossRef]
29. Jasinski, F.; Zetterlund, P.B.; Braun, A.M.; Chemtob, A. Photopolymerization in dispersed systems. *Prog. Polym. Sci.* **2018**, *84*, 47–88. [CrossRef]
30. Noè, C.; Hakkarainen, M.; Sangermano, M. Cationic UV-Curing of Epoxidized Biobased Resins. *Polymers* **2021**, *13*, 89. [CrossRef]
31. Yuan, Y.; Li, C.; Zhang, R.; Liu, R.; Liu, J. Low volume shrinkage photopolymerization system using hydrogen-bond-based monomers. *Prog. Org. Coat.* **2019**, *137*, 105308. [CrossRef]
32. Khudyakov, I.V.; Legg, J.C.; Purvis, M.B.; Overton, B.J. Kinetics of Photopolymerization of Acrylates with Functionality of 1-6. *Ind. Eng. Chem. Res.* **1999**, *38*, 3353–3359. [CrossRef]
33. Noirbent, G.; Dumur, F. Photoinitiators of polymerization with reduced environmental impact: Nature as an unlimited and renewable source of dyes. *Eur. Polym. J.* **2021**, *142*, 110109. [CrossRef]
34. Zhao, H.; Sha, J.; Wang, X.; Jiang, Y.; Chen, T.; Wu, T.; Chen, X.; Ji, H.; Gao, Y.; Xie, L.; et al. Spatiotemporal control of polymer brush formation through photoinduced radical polymerization regulated by DMD light modulation. *Lab Chip* **2019**, *19*, 2651–2662. [CrossRef] [PubMed]
35. Xi, W.; Peng, H.; Aguirre-Soto, A.; Kloxin, C.J.; Stansbury, J.W.; Bowman, C.N. Spatial and Temporal Control of Thiol-Michael Addition via Photocaged Superbase in Photopatterning and Two-Stage Polymer Networks Formation. *Macromolecules* **2014**, *47*, 6159–6165. [CrossRef]
36. Tehfe, M.-A.; Dumur, F.; Contal, E.; Graff, B.; Gigmes, D.; Fouassier, J.-P.; Lalevée, J. Novel highly efficient organophotocatalysts: Truxene-acridine-1,8-diones as photoinitiators of polymerization. *Macromol. Chem. Phys.* **2013**, *214*, 2189–2201. [CrossRef]
37. Xiao, P.; Dumur, F.; Tehfe, M.-A.; Graff, B.; Gigmes, D.; Fouassier, J.-P.; Lalevée, J. Difunctional acridinediones as photoinitiators of polymerization under UV and visible lights: Structural effects. *Polymer* **2013**, *54*, 3458–3466. [CrossRef]
38. Xiao, P.; Dumur, F.; Tehfe, M.-A.; Graff, B.; Gigmes, D.; Fouassier, J.-P.; Lalevée, J. Acridinediones: Effect of substituents on their photoinitiating abilities in radical and cationic photopolymerization. *Macromol. Chem. Phys.* **2013**, *214*, 2276–2282. [CrossRef]
39. Zhang, J.; Campolo, D.; Dumur, F.; Xiao, P.; Gigmes, D.; Fouassier, J.-P.; Lalevée, J. The carbazole-bound ferrocenium salt as a specific cationic photoinitiator upon near-UV and visible LEDs (365–405 nm). *Polym. Bull.* **2016**, *73*, 493–507. [CrossRef]
40. Al Mousawi, A.; Dumur, F.; Toufaily, J.; Hamieh, T.; Graff, B.; Gigmes, D.; Fouassier, J.-P.; Lalevée, J. Carbazole scaffold based photoinitiators/photoredox catalysts for new LED projector 3D printing resins. *Macromolecules* **2017**, *50*, 2747–2758. [CrossRef]
41. Al Mousawi, A.; Magaldi Lara, D.; Noirbent, G.; Dumur, F.; Toufaily, J.; Hamieh, T.; Bui, T.-T.; Goubard, F.; Graff, B.; Gigmes, D.; et al. Carbazole derivatives with thermally activated delayed fluorescence property as photoinitiators/photoredox catalysts for LED 3D printing technology. *Macromolecules* **2017**, *50*, 4913–4926. [CrossRef]
42. Al Mousawi, A.; Garra, P.; Dumur, F.; Bui, T.-T.; Goubard, F.; Toufaily, J.; Hamieh, T.; Graff, B.; Gigmes, D.; Fouassier, J.-P.; et al. Novel Carbazole Skeleton-Based Photoinitiators for LED Polymerization and LED Projector 3D Printing. *Molecules* **2018**, *22*, 2143. [CrossRef]
43. Al Mousawi, A.; Arar, A.; Ibrahim-Ouali, M.; Duval, S.; Dumur, F.; Garra, P.; Toufaily, J.; Hamieh, T.; Graff, B.; Gigmes, D.; et al. Carbazole-based compounds as photoinitiators for free radical and cationic polymerization upon near visible light illumination. *Photochem. Photobiol. Sci.* **2018**, *17*, 578–585. [CrossRef]
44. Abdallah, M.; Magaldi, D.; Hijazi, A.; Graff, B.; Dumur, F.; Fouassier, J.-P.; Bui, T.-T.; Goubard, F.; Lalevée, J. Development of new high performance visible light photoinitiators based on carbazole scaffold and their applications in 3D printing and photocomposite synthesis. *J. Polym. Sci. A Polym. Chem.* **2019**, *57*, 2081–2092. [CrossRef]
45. Tehfe, M.-A.; Dumur, F.; Contal, E.; Graff, B.; Gigmes, D.; Morlet-Savary, F.; Fouassier, J.-P.; Lalevée, J. New insights in radical and cationic polymerizations upon visible light exposure: Role of novel photoinitiator systems based on the pyrene chromophore. *Polym. Chem.* **2013**, *4*, 1625–1634. [CrossRef]
46. Telitel, S.; Dumur, F.; Faury, T.; Graff, B.; Tehfe, M.-A.; Gigmes, D.; Fouassier, J.-P.; Lalevée, J. New core-pyrene π-structure organophotocatalysts usable as highly efficient photoinitiators. *Beilstein J. Org. Chem.* **2013**, *9*, 877–890. [CrossRef] [PubMed]
47. Uchida, N.; Nakano, H.; Igarashi, T.; Sakurai, T. Nonsalt 1-(arylmethyloxy)pyrene photoinitiators capable of initiating cationic polymerization. *J. Appl. Polym. Sci.* **2014**, *131*, 40510. [CrossRef]
48. Mishra, A.; Daswal, S. 1-(Bromoacetyl)pyrene, a novel photoinitiator for the copolymerization of styrene and methylmethacrylate. *Rad. Phys. Chem.* **2006**, *75*, 1093–1100. [CrossRef]
49. Tehfe, M.-A.; Dumur, F.; Graff, B.; Morlet-Savary, F.; Gigmes, D.; Fouassier, J.-P.; Lalevée, J. Design of new Type I & Type II photoinitiators possessing highly coupled pyrene-ketone moieties. *Polym. Chem.* **2013**, *4*, 2313–2324.
50. Dumur, F. Recent advances on pyrene-based photoinitiators of polymerization. *Eur. Polym. J.* **2020**, *126*, 109564. [CrossRef]
51. Lalevée, J.; Peter, M.; Dumur, F.; Gigmes, D.; Blanchard, N.; Tehfe, M.-A.; Morlet-Savary, F.; Fouassier, J.-P. Subtle ligand effects in oxidative photocatalysis with iridium complexes: Application to photopolymerization. *Chem. Eur. J.* **2011**, *17*, 15027–15031. [CrossRef]

52. Lalevée, J.; Tehfe, M.-A.; Dumur, F.; Gigmes, D.; Blanchard, N.; Morlet-Savary, F.; Fouassier, J.-P. Iridium photocatalysts in free radical photopolymerization under visible lights. *ACS Macro Lett.* **2012**, *1*, 286–290. [CrossRef]
53. Lalevée, J.; Dumur, F.; Mayer, C.R.; Gigmes, D.; Nasr, G.; Tehfe, M.-A.; Telitel, S.; Morlet-Savary, F.; Graff, B.; Fouassier, J.-P. Photopolymerization of N-vinylcarbazole using visible-light harvesting iridium complexes as photoinitiators. *Macromolecules* **2012**, *45*, 4134–4141. [CrossRef]
54. Telitel, S.; Dumur, F.; Telitel, S.; Soppera, O.; Lepeltier, M.; Guillaneuf, Y.; Poly, J.; Morlet-Savary, F.; Fioux, P.; Fouassier, J.-P.; et al. Photoredox catalysis using a new iridium complex as an efficient toolbox for radical, cationic and controlled polymerizations under soft blue to green lights. *Polym. Chem.* **2015**, *6*, 613–624. [CrossRef]
55. Telitel, S.; Dumur, F.; Lepeltier, M.; Gigmes, D.; Fouassier, J.-P.; Lalevée, J. Photoredox process induced polymerization reactions: Iridium complexes for panchromatic photo-initiating systems. *C. R. Chim.* **2016**, *19*, 71–78. [CrossRef]
56. Tehfe, M.-A.; Lepeltier, M.; Dumur, F.; Gigmes, D.; Fouassier, J.-P.; Lalevée, J. Structural effects in the iridium complex series: Photoredox catalysis and photoinitiation of polymerization reactions under visible lights. *Macromol. Chem. Phys.* **2017**, *218*, 1700192. [CrossRef]
57. Dumur, F.; Nasr, G.; Wantz, G.; Mayer, C.R.; Dumas, E.; Guerlin, A.; Miomandre, F.; Clavier, G.; Bertin, D.; Gigmes, D. Cationic iridium complex for the design of soft salt-based phosphorescent OLEDs and color-tunable Light-Emitting Electrochemical Cells. *Org. Electron.* **2011**, *12*, 1683–1694. [CrossRef]
58. Nasr, G.; Guerlin, A.; Dumur, F.; Beouch, L.; Dumas, E.; Clavier, G.; Miomandre, F.; Goubard, F.; Gigmes, D.; Bertin, D.; et al. Iridium (III) soft salts from dinuclear cationic and mononuclear anionic complexes for OLEDs devices. *Chem. Commun.* **2011**, *47*, 10698–10700. [CrossRef] [PubMed]
59. Dumur, F.; Bertin, D.; Gigmes, D. Iridium (III) complexes as promising emitters for solid-state light-emitting electrochemical cells (LECs). *Int. J. Nanotechnol.* **2012**, *9*, 377–395. [CrossRef]
60. Xiao, P.; Dumur, F.; Zhang, J.; Fouassier, J.-P.; Gigmes, D.; Lalevée, J. Copper complexes in radical photoinitiating systems: Applications to free radical and cationic polymerization under visible lights. *Macromolecules* **2014**, *47*, 3837–3844. [CrossRef]
61. Xiao, P.; Dumur, F.; Zhang, J.; Gigmes, D.; Fouassier, J.-P.; Lalevée, J. Copper complexes: The effect of ligands on their photoinitiation efficiencies in radical polymerization reactions under visible light. *Polym. Chem.* **2014**, *5*, 6350–6357. [CrossRef]
62. Xiao, P.; Zhang, J.; Campolo, D.; Dumur, F.; Gigmes, D.; Fouassier, J.-P.; Lalevée, J. Copper and iron complexes as visible-light-sensitive photoinitiators of polymerization. *J. Polym. Sci. A Polym. Chem.* **2015**, *53*, 2673–2684. [CrossRef]
63. Al Mousawi, A.; Kermagoret, A.; Versace, D.-L.; Toufaily, J.; Hamieh, T.; Graff, B.; Dumur, F.; Gigmes, D.; Fouassier, J.-P.; Lalevée, J. Copper photoredox catalysts for polymerization upon near UV or visible light: Structure/reactivity/ efficiency relationships and use in LED projector 3D printing resins. *Polym. Chem.* **2017**, *8*, 568–580. [CrossRef]
64. Garra, P.; Kermagoret, A.; Al Mousawi, A.; Dumur, F.; Gigmes, D.; Morlet-Savary, F.; Dietlin, C.; Fouassier, J.-P.; Lalevée, J. New copper(I) complex based initiating systems in redox polymerization and comparison with the amine/benzoyl peroxide reference. *Polym. Chem.* **2017**, *8*, 4088–4097. [CrossRef]
65. Garra, P.; Dumur, F.; Morlet-Savary, F.; Dietlin, C.; Gigmes, D.; Fouassier, J.-P.; Lalevée, J. Mechanosynthesis of a copper complex for redox initiating systems with a unique near infrared light activation. *J. Polym. Sci. A Polym. Chem.* **2017**, *55*, 3646–3655. [CrossRef]
66. Mokbel, H.; Anderson, D.; Plenderleith, R.; Dietlin, C.; Morlet-Savary, F.; Dumur, F.; Gigmes, D.; Fouassier, J.-P.; Lalevée, J. Copper PhotoRedox Catalyst "G1": A New High Performance Photoinitiator for Near-UV and Visible LEDs. *Polym. Chem.* **2017**, *8*, 5580–5592. [CrossRef]
67. Garra, P.; Dumur, F.; Al Mousawi, A.; Graff, B.; Gigmes, D.; Morlet-Savary, F.; Dietlin, C.; Fouassier, J.-P.; Lalevée, J. Mechanosynthesized Copper (I) complex based initiating systems for redox polymerization: Towards upgraded oxidizing and reducing agents. *Polym. Chem.* **2017**, *8*, 5884–5896. [CrossRef]
68. Garra, P.; Carré, M.; Dumur, F.; Morlet-Savary, F.; Dietlin, C.; Gigmes, D.; Fouassier, J.-P.; Lalevée, J. Copper-based (photo) redox initiating systems as highly efficient systems for interpenetrating polymer network preparation. *Macromolecules* **2018**, *51*, 679–688. [CrossRef]
69. Garra, P.; Dumur, F.; Nechab, M.; Morlet-Savary, F.; Dietlin, C.; Graff, B.; Gigmes, D.; Fouassier, J.-P.; Lalevée, J. Stable copper acetylacetonate-based oxidizing agents in redox (NIR photoactivated) polymerization: An opportunity for one pot grafting from approach and example on a 3D printed object. *Polym. Chem.* **2018**, *9*, 2173–2182. [CrossRef]
70. Mokbel, H.; Anderson, D.; Plenderleith, R.; Dietlin, C.; Morlet-Savary, F.; Dumur, F.; Gigmes, D.; Fouassier, J.-P.; Lalevée, J. Simultaneous initiation of radical and cationic polymerization reactions using the "G1" copper complex as photoRedox catalyst: Applications of free radical/cationic hybrid photo-polymerization in the composites and 3D printing fields. *Prog. Org. Coat.* **2019**, *132*, 50–61. [CrossRef]
71. Launay, V.; Caron, A.; Noirbent, G.; Gigmes, D.; Dumur, F.; Lalevée, J. NIR dyes as innovative tools for reprocessing/recycling of plastics: Benefits of the photothermal activation in the near-infrared range. *Adv. Funct. Mater.* **2021**, *31*, 2006324. [CrossRef]
72. Bonardi, A.; Bonardi, F.; Noirbent, G.; Dumur, F.; Dietlin, C.; Gigmes, D.; Fouassier, J.-P.; Lalevée, J. Different NIR dye scaffolds for polymerization reactions under NIR light. *Polym. Chem.* **2019**, *10*, 6505–6514. [CrossRef]
73. Giacoletto, N.; Ibrahim-Ouali, M.; Dumur, F. Recent advances on squaraine-based photoinitiators of polymerization. *Eur. Polym. J.* **2021**, *150*, 110427. [CrossRef]

74. Kamoun, E.A.; Winkel, A.; Eisenburger, M.; Menzel, H. Carboxylated camphorquinone as visible-light photoinitiator for biomedical application: Synthesis, characterization, and application. *Arab. J. Chem.* **2016**, *9*, 745–754. [CrossRef]
75. Santini, A.; Gallegos, I.T.; Felix, C.M. Photoinitiators in dentistry: A review. *Prim. Dent. J.* **2013**, *2*, 30–33. [CrossRef]
76. Xiao, P.; Dumur, F.; Frigoli, M.; Graff, B.; Morlet-Savary, F.; Wantz, G.; Bock, H.; Fouassier, J.-P.; Gigmes, D.; Lalevée, J. Perylene derivatives as photoinitiators in blue light sensitive cationic or radical curable films and panchromatic thiol-ene polymerizable films. *Eur. Polym. J.* **2014**, *53*, 215–222. [CrossRef]
77. Tehfe, M.-A.; Dumur, F.; Graff, B.; Gigmes, D.; Fouassier, J.-P.; Lalevée, J. Green light induced cationic ring opening polymerization reactions: Perylene-3,4:9,10-bis(dicarboximide) as efficient photosensitizers. *Macromol. Chem. Phys.* **2013**, *214*, 1052–1060. [CrossRef]
78. Xiao, P.; Dumur, F.; Graff, B.; Gigmes, D.; Fouassier, J.-P.; Lalevée, J. Red-light-induced cationic photopolymerization: Perylene derivatives as efficient photoinitiators. Macromol. *Rapid Commun.* **2013**, *34*, 1452–1458. [CrossRef]
79. Mokbel, H.; Toufaily, J.; Hamieh, T.; Dumur, F.; Campolo, D.; Gigmes, D.; Fouassier, J.-P.; Ortyl, J.; Lalevee, J. Specific cationic photoinitiators for Near UV and visible LEDs: Iodonium vs. ferrocenium structures. *J. Appl. Polym. Sci.* **2015**, *132*, 42759. [CrossRef]
80. Villotte, S.; Gigmes, D.; Dumur, F.; Lalevée, J. Design of Iodonium Salts for UV or Near-UV LEDs for Photoacid Generator and Polymerization Purposes. *Molecules* **2020**, *25*, 149. [CrossRef]
81. Zivic, N.; Bouzrati-Zerrelli, M.; Villotte, S.; Morlet-Savary, F.; Dietlin, C.; Dumur, F.; Gigmes, D.; Fouassier, J.-P.; Lalevée, J. A novel naphthalimide scaffold based iodonium salt as a one-component photoacid/photoinitiator for cationic and radical polymerization under LED exposure. *Polym. Chem.* **2016**, *7*, 5873–5879. [CrossRef]
82. Liu, S.; Chen, H.; Zhang, Y.; Sun, K.; Xu, Y.; Morlet-Savary, F.; Graff, B.; Noirbent, G.; Pigot, C.; Brunel, D.; et al. Monocomponent photoinitiators based on benzophenone-carbazole structure for led photoinitiating systems and application on 3D printing. *Polymers* **2020**, *12*, 1394. [CrossRef] [PubMed]
83. Xiao, P.; Dumur, F.; Graff, B.; Gigmes, D.; Fouassier, J.-P.; Lalevée, J. Variations on the benzophenone skeleton: Novel high-performance blue light sensitive photoinitiating systems. *Macromolecules* **2013**, *46*, 7661–7667. [CrossRef]
84. Zhang, J.; Frigoli, M.; Dumur, F.; Xiao, P.; Ronchi, L.; Graff, B.; Morlet-Savary, F.; Fouassier, J.-P.; Gigmes, D.; Lalevée, J. Design of novel photoinitiators for radical and cationic photopolymerizations under Near UV and Visible LEDs (385, 395 and 405 nm). *Macromolecules* **2014**, *47*, 2811–2819. [CrossRef]
85. Liu, S.; Brunel, D.; Noirbent, G.; Mau, A.; Chen, H.; Morlet-Savary, F.; Graff, B.; Gigmes, D.; Xiao, P.; Dumur, F.; et al. New multifunctional benzophenone-based photoinitiators with high migration stability and their application in 3D printing. *Mater. Chem. Front.* **2021**, *5*, 1982–1994. [CrossRef]
86. Liu, S.; Brunel, D.; Sun, K.; Zhang, Y.; Chen, H.; Xiao, P.; Dumur, F.; Lalevée, J. Novel photoinitiators based on benzophenone-triphenylamine hybrid structure for led photopolymerization. *Macromol. Rapid Commun.* **2020**, *41*, 2000460. [CrossRef]
87. Liu, S.; Brunel, D.; Sun, K.; Xu, Y.; Morlet-Savary, F.; Graff, B.; Xiao, P.; Dumur, F.; Lalevée, J. A mono-component bifunctional benzophenone-carbazole type II photoinitiator for led photoinitiating systems. *Polym. Chem.* **2020**, *11*, 3551–3556. [CrossRef]
88. Mokbel, H.; Dumur, F.; Lalevée, J. On demand NIR activated photopolyaddition reactions. *Polym. Chem.* **2020**, *11*, 4250–4259. [CrossRef]
89. Mokbel, H.; Graff, B.; Dumur, F.; Lalevée, J. NIR sensitizer operating under long wavelength (1064 nm) for free radical photopolymerization processes. *Macromol. Rapid Commun.* **2020**, *41*, 2000289. [CrossRef]
90. Zhang, J.; Zivic, N.; Dumur, F.; Guo, C.; Li, Y.; Xiao, P.; Graff, B.; Gigmes, D.; Fouassier, J.-P.; Lalevée, J. Panchromatic photoinitiators for radical, cationic and thiol-ene polymerization reactions: A search in the diketopyrrolopyrrole or indigo dye series. *Mater. Today Commun.* **2015**, *4*, 101–108. [CrossRef]
91. Xiao, P.; Hong, W.; Li, Y.; Dumur, F.; Graff, B.; Fouassier, J.-P.; Gigmes, D.; Lalevée, J. Diketopyrrolopyrrole dyes: Structure/reactivity/efficiency relationship in photoinitiating systems upon visible lights. *Polymer* **2014**, *55*, 746–751. [CrossRef]
92. Xiao, P.; Hong, W.; Li, Y.; Dumur, F.; Graff, B.; Fouassier, J.-P.; Gigmes, D.; Lalevée, J. Green light sensitive diketopyrrolopyrrole derivatives used in versatile photoinitiating systems for photopolymerizations. *Polym. Chem.* **2014**, *5*, 2293–2300. [CrossRef]
93. Al Mousawi, A.; Dumur, F.; Garra, P.; Toufaily, J.; Hamieh, T.; Goubard, F.; Bui, T.-T.; Graff, B.; Gigmes, D.; Fouassier, J.-P.; et al. Azahelicenes as visible light photoinitiators for cationic and radical polymerization: Preparation of photo-luminescent polymers and use in high performance LED projector 3D printing resins. *J. Polym. Sci. A Polym. Chem.* **2017**, *55*, 1189–1199. [CrossRef]
94. Al Mousawi, A.; Schmitt, M.; Dumur, F.; Ouyang, J.; Favereaud, L.; Dorcet, V.; Vanthuyne, N.; Garra, P.; Toufaily, J.; Hamieh, T.; et al. Visible light chiral photoinitiator for radical polymerization and synthesis of polymeric films with strong chiroptical activity. *Macromolecules* **2018**, *51*, 5628–5637. [CrossRef]
95. Bonardi, A.-H.; Zahouily, S.; Dietlin, C.; Graff, B.; Morlet-Savary, F.; Ibrahim-Ouali, M.; Gigmes, D.; Hoffmann, N.; Dumur, F.; Lalevée, J. New 1,8-naphthalimide derivatives as photoinitiators for free radical polymerization upon visible light. *Catalysts* **2019**, *9*, 637. [CrossRef]
96. Zhang, J.; Zivic, N.; Dumur, F.; Xiao, P.; Graff, B.; Fouassier, J.-P.; Gigmes, D.; Lalevée, J. Naphthalimide-tertiary amine derivatives as blue-light-sensitive photoinitiators. *ChemPhotoChem* **2018**, *2*, 481–489. [CrossRef]
97. Xiao, P.; Dumur, F.; Zhang, J.; Graff, B.; Gigmes, D.; Fouassier, J.-P.; Lalevée, J. Naphthalimide derivatives: Substituent effects on the photoinitiating ability in polymerizations under near UV, purple, white and blue LEDs (385 nm, 395 nm, 405 nm, 455 nm or 470 nm). *Macromol. Chem. Phys.* **2015**, *216*, 1782–1790. [CrossRef]

98. Xiao, P.; Dumur, F.; Zhang, J.; Graff, B.; Gigmes, D.; Fouassier, J.-P.; Lalevée, J. Naphthalimide-phthalimide derivative based photoinitiating systems for polymerization reactions under blue lights. *J. Polym. Sci. A Polym. Chem.* **2015**, *53*, 665–674. [CrossRef]
99. Zhang, J.; Zivic, N.; Dumur, F.; Xiao, P.; Graff, B.; Gigmes, D.; Fouassier, J.-P.; Lalevée, J. A benzophenone-naphthalimide derivative as versatile photoinitiator for near UV and visible lights. *J. Polym. Sci. A Polym. Chem.* **2015**, *53*, 445–451. [CrossRef]
100. Zhang, J.; Zivic, N.; Dumur, F.; Xiao, P.; Graff, B.; Fouassier, J.-P.; Gigmes, D.; Lalevée, J. N-[2-(dimethylamino)ethyl]-1,8-naphthalimide derivatives as photoinitiators under LEDs. *Polym. Chem.* **2018**, *9*, 994–1003. [CrossRef]
101. Zivic, N.; Zhang, J.; Bardelang, D.; Dumur, F.; Xiao, P.; Jet, T.; Versace, D.-L.; Dietlin, C.; Morlet-Savary, F.; Graff, B.; et al. Novel naphthalimideamine based photoinitiators operating under violet and blue LEDs and usable for various polymerization reactions and synthesis of hydrogels. *Polym. Chem.* **2016**, *7*, 418–429. [CrossRef]
102. Zhang, J.; Dumur, F.; Xiao, P.; Graff, B.; Bardelang, D.; Gigmes, D.; Fouassier, J.-P.; Lalevée, J. Structure design of naphthalimide derivatives: Towards versatile photo-initiators for near UV/Visible LEDs, 3D printing and water-soluble photoinitiating systems. *Macromolecules* **2015**, *48*, 2054–2063. [CrossRef]
103. Zhang, J.; Zivic, N.; Dumur, F.; Xiao, P.; Graff, B.; Fouassier, J.-P.; Gigmes, D.; Lalevée, J. UV violet-blue LED induced polymerizations: Specific photoinitiating systems at 365, 385, 395 and 405 nm. *Polymer* **2014**, *55*, 6641–6648. [CrossRef]
104. Xiao, P.; Dumur, F.; Graff, B.; Gigmes, D.; Fouassier, J.-P.; Lalevée, J. Blue light sensitive dyes for various photopolymerization reactions: Naphthalimide and naphthalic anhydride derivatives. *Macromolecules* **2014**, *47*, 601–608. [CrossRef]
105. Xiao, P.; Dumur, F.; Frigoli, M.; Tehfe, M.-A.; Graff, B.; Fouassier, J.-P.; Gigmes, D.; Lalevée, J. Naphthalimide based methacrylated photoinitiators in radical and cationic photopolymerization under visible light. *Polym. Chem.* **2013**, *4*, 5440–5448. [CrossRef]
106. Noirbent, G.; Dumur, F. Recent advances on naphthalic anhydrides and 1,8-naphthalimide-based photoinitiators of polymerization. *Eur. Polym. J.* **2020**, *132*, 109702. [CrossRef]
107. Rahal, M.; Mokbel, H.; Graff, B.; Pertici, V.; Gigmes, D.; Toufaily, J.; Hamieh, T.; Dumur, F.; Lalevée, J. Naphthalimide-Based dyes as photoinitiators under visible light irradiation and their applications: Photocomposite synthesis, 3D printing and polymerization in water. *ChemPhotoChem* **2021**, *5*, 476–490. [CrossRef]
108. Chen, H.; Noirbent, G.; Sun, K.; Brunel, D.; Gigmes, D.; Morlet-Savary, F.; Zhang, Y.; Liu, S.; Xiao, P.; Dumur, F.; et al. Photoinitiators derived from natural product scaffolds: Mono-chalcones in three-component photoinitiating systems and their applications in 3D printing. *Polym. Chem.* **2020**, *11*, 4647–4659. [CrossRef]
109. Tang, L.; Nie, J.; Zhu, X. A high-performance phenyl-free LED photoinitiator for cationic or hybrid photopolymerization and its application in LED cationic 3D printing. *Polym. Chem.* **2020**, *11*, 2855–2863. [CrossRef]
110. Xu, Y.; Noirbent, G.; Brunel, D.; Ding, Z.; Gigmes, D.; Graff, B.; Xiao, P.; Dumur, F.; Lalevée, J. Allyloxy ketones as efficient photoinitiators with high migration stability in free radical polymerization and 3D printing. *Dyes Pigm.* **2021**, *185*, 108900. [CrossRef]
111. Sun, K.; Chen, H.; Zhang, Y.; Morlet-Savary, F.; Graff, B.; Xiao, P.; Dumur, F.; Lalevée, J. High-performance sunlight induced polymerization using novel push-pull dyes with high light absorption properties. *Eur. Polym. J.* **2021**, *151*, 110410. [CrossRef]
112. Chen, H.; Noirbent, G.; Liu, S.; Brunel, D.; Graff, B.; Gigmes, D.; Zhang, Y.; Sun, K.; Morlet-Savary, F.; Xiao, P.; et al. Bis-chalcone derivatives derived from natural products as near-UV/visible light sensitive photoinitiators for 3D/4D printing. *Mater. Chem. Front.* **2021**, *5*, 901–916. [CrossRef]
113. Xu, Y.; Ding, Z.; Zhu, H.; Graff, B.; Xiao, P.; Dumur, F.; Lalevée, F. Design of ketone derivatives as highly efficient photoinitiators for free radical and cationic photopolymerizations and application in 3D printing of composites. *J. Polym. Sci.* **2021**. [CrossRef]
114. Liu, S.; Zhang, Y.; Sun, K.; Graff, B.; Xiao, P.; Dumur, F.; Lalevée, J. Design of photoinitiating systems based on the chalcone-anthracene scaffold for led cationic photopolymerization and application in 3D Printing. *Eur. Polym. J.* **2021**, *147*, 110300. [CrossRef]
115. Zhang, J.; Campolo, D.; Dumur, F.; Xiao, P.; Fouassier, J.-P.; Gigmes, D.; Lalevée, J. Iron complexes as photoinitiators for radical and cationic polymerization through photoredox catalysis processes. *J. Polym. Sci. A Polym. Chem.* **2015**, *53*, 42–49. [CrossRef]
116. Telitel, S.; Dumur, F.; Campolo, D.; Poly, J.; Gigmes, D.; Fouassier, J.-P.; Lalevée, J. Iron complexes as potential photocatalysts for controlled radical photopolymerizations: A tool for modifications and patterning of surfaces. *J. Polym. Sci. A Polym. Chem.* **2016**, *54*, 702–713. [CrossRef]
117. Zhang, J.; Campolo, D.; Dumur, F.; Xiao, P.; Fouassier, J.-P.; Gigmes, D.; Lalevée, J. Visible-light-sensitive photoredox catalysis by iron complexes: Applications in cationic and radical polymerization reactions. *J. Polym. Sci. A Polym. Chem.* **2016**, *54*, 2247–2253. [CrossRef]
118. Zhang, J.; Campolo, D.; Dumur, F.; Xiao, P.; Fouassier, J.-P.; Gigmes, D.; Lalevée, J. Novel iron complexes in visible-light-sensitive photoredox catalysis: Effect of ligands on their photoinitiation efficiencies. *ChemCatChem* **2016**, *8*, 2227–2233. [CrossRef]
119. Zhang, J.; Dumur, F.; Horcajada, P.; Livage, C.; Xiao, P.; Fouassier, J.-P.; Gigmes, D.; Lalevée, J. Iron-based metal-organic frameworks (MOF) as photocatalysts for radical and cationic polymerizations under near UV and visible LEDs (385–405 nm). *Macromol. Chem. Phys.* **2016**, *217*, 2534–2540. [CrossRef]
120. Dumur, F. Recent advances on ferrocene-based photoinitiating systems. *Eur. Polym. J.* **2021**, *147*, 110328. [CrossRef]
121. Tehfe, M.-A.; Dumur, F.; Xiao, P.; Graff, B.; Morlet-Savary, F.; Fouassier, J.-P.; Gigmes, D.; Lalevée, J. New chromone based photoinitiators for polymerization reactions upon visible lights. *Polym. Chem.* **2013**, *4*, 4234–4244. [CrossRef]
122. You, J.; Fu, H.; Zhao, D.; Hu, T.; Nie, J.; Wang, T. Flavonol dyes with different substituents in photopolymerization. *J. Photochem. Photobiol. A Chem.* **2020**, *386*, 112097. [CrossRef]

123. Al Mousawi, A.; Garra, P.; Schmitt, M.; Toufaily, J.; Hamieh, T.; Graff, B.; Fouassier, J.-P.; Dumur, F.; Lalevée, J. 3-Hydroxyflavone and N-phenyl-glycine in high performance photo-initiating systems for 3D printing and photocomposites synthesis. *Macromolecules* **2018**, *51*, 4633–4641. [CrossRef]
124. Karaca, N.; Ocala, N.; Arsua, N.; Jockusch, S. Thioxanthone-benzothiophenes as photoinitiator for free radical polymerization. *J. Photochem. Photobiol. A Chem.* **2016**, *331*, 22–28. [CrossRef]
125. Wu, Q.; Wang, X.; Xiong, Y.; Yang, J.; Tang, H. Thioxanthone based one-component polymerizable visible light photoinitiator for free radical polymerization. *RSC Adv.* **2016**, *6*, 66098–66107. [CrossRef]
126. Qiu, J.; Wei, J. Thioxanthone photoinitiator containing polymerizable N-aromatic maleimide for photopolymerization. *J. Polym. Res.* **2014**, *21*, 559. [CrossRef]
127. Dadashi-Silab, S.; Aydogan, C.; Yagci, Y. Shining a light on an adaptable photoinitiator: Advances in photopolymerizations initiated by thioxanthones. *Polym. Chem.* **2015**, *6*, 6595–6615. [CrossRef]
128. Zhang, J.; Lalevée, J.; Zhao, J.; Graff, B.; Stenzel, M.H.; Xiao, P. Dihydroxyanthraquinone derivatives: Natural dyes as blue-light-sensitive versatile photoinitiators of photopolymerization. *Polym. Chem.* **2016**, *7*, 7316–7324. [CrossRef]
129. Al Mousawi, A.; Poriel, C.; Dumur, F.; Toufaily, J.; Hamieh, T.; Fouassier, J.-P.; Lalevée, J. Zinc tetraphenylporphyrin as high performance visible-light photoinitiator of cationic photosensitive resins for LED projector 3D printing applications. *Macromolecules* **2017**, *50*, 746–753. [CrossRef]
130. Noirbent, G.; Xu, Y.; Bonardi, A.-H.; Gigmes, D.; Lalevée, J.; Dumur, F. Metalated Porphyrins as versatile visible light and NIR photoinitiators of polymerization. *Eur. Polym. J.* **2020**, *139*, 110019. [CrossRef]
131. Tehfe, M.-A.; Lalevée, J.; Dumur, F.; Telitel, S.; Gigmes, D.; Contal, E.; Bertin, D.; Fouassier, J.-P. Zinc-based metal complexes as new photocatalysts in polymerization initiating systems. *Eur. Polym. J.* **2013**, *49*, 1040–1049. [CrossRef]
132. Abdallah, M.; Le, H.; Hijazi, A.; Graff, B.; Dumur, F.; Bui, T.-T.; Goubard, F.; Fouassier, J.-P.; Lalevée, J. Acridone derivatives as high performance visible light photoinitiators for cationic and radical photosensitive resins for 3D printing technology and for low migration photopolymer property. *Polymer* **2018**, *159*, 47–58. [CrossRef]
133. Zhang, J.; Dumur, F.; Bouzrati, M.; Xiao, P.; Dietlin, C.; Morlet-Savary, F.; Graff, B.; Gigmes, D.; Fouassier, J.-P.; Lalevée, J. Novel panchromatic photopolymerizable matrices: N,N′-dibutyl-quinacridone as an efficient and versatile photoinitiator. *J. Polym. Sci. A Polym. Chem.* **2015**, *53*, 1719–1727. [CrossRef]
134. Tehfe, M.-A.; Zein-Fakih, A.; Lalevée, J.; Dumur, F.; Gigmes, D.; Graff, B.; Morlet-Savary, F.; Hamieh, T.; Fouassier, J.-P. New pyridinium salts as versatile compounds for dye sensitized photo-polymerization. *Eur. Polym. J.* **2013**, *49*, 567–574. [CrossRef]
135. Xiao, P.; Frigoli, M.; Dumur, F.; Graff, B.; Gigmes, D.; Fouassier, J.-P.; Lalevée, J. Julolidine or fluorenone based push-pull dyes for polymerization upon soft polychromatic visible light or green light. *Macromolecules* **2014**, *47*, 106–112. [CrossRef]
136. Tehfe, M.-A.; Dumur, F.; Graff, B.; Morlet-Savary, F.; Fouassier, J.-P.; Gigmes, D.; Lalevée, J. New push-pull dyes derived from Michler's ketone for polymerization reactions upon visible lights. *Macromolecules* **2013**, *46*, 3761–3770. [CrossRef]
137. Mokbel, H.; Dumur, F.; Mayer, C.R.; Morlet-Savary, F.; Graff, B.; Gigmes, D.; Toufaily, J.; Hamieh, T.; Fouassier, J.-P.; Lalevée, J. End capped polyenic structures as visible light sensitive photoinitiators for polymerization of vinylethers. *Dyes Pigm.* **2014**, *105*, 121–129. [CrossRef]
138. Garra, P.; Brunel, D.; Noirbent, G.; Graff, B.; Morlet-Savary, F.; Dietlin, C.; Sidorkin, V.F.; Dumur, F.; Duché, D.; Gigmes, D.; et al. Ferrocene-based (photo)redox polymerization under long wavelengths. *Polym. Chem.* **2019**, *10*, 1431–1441. [CrossRef]
139. Telitel, S.; Dumur, F.; Kavalli, T.; Graff, B.; Morlet-Savary, F.; Gigmes, D.; Fouassier, J.-P.; Lalevée, J. The 1,3-bis(dicyanomethylidene)-indane skeleton as a (photo) initiator in thermal ring opening polymerization at RT and radical or cationic photopolymerization. *RSC Adv.* **2014**, *4*, 15930–15936. [CrossRef]
140. Mokbel, H.; Dumur, F.; Graff, B.; Mayer, C.R.; Gigmes, D.; Toufaily, J.; Hamieh, T.; Fouassier, J.-P.; Lalevée, J. Michler's ketone as an interesting scaffold for the design of high-performance dyes in photoinitiating systems upon visible lights. *Macromol. Chem. Phys.* **2014**, *215*, 783–790. [CrossRef]
141. Sun, K.; Liu, S.; Pigot, S.; Brunel, D.; Graff, B.; Nechab, M.; Gigmes, D.; Morlet-Savary, F.; Zhang, Y.; Xiao, P.; et al. Novel push-pull dyes derived from 1H-cyclopenta[b]naphthalene-1,3(2H)-dione as versatile photoinitiators for photopolymerization and their related applications: 3D-printing and fabrication of photocomposites. *Catalysts* **2020**, *10*, 1196. [CrossRef]
142. Tehfe, M.-A.; Dumur, F.; Graff, B.; Morlet-Savary, F.; Gigmes, D.; Fouassier, J.-P.; Lalevée, J. Push–pull (thio)barbituric acid derivatives in dye photosensitized radical and cationic polymerization reactions under 457/473 nm laser beams or blue LEDs. *Polym. Chem.* **2013**, *4*, 3866–3875. [CrossRef]
143. Dumur, F.; Gigmes, D.; Fouassier, J.-P.; Lalevée, J. Organic Electronics: An El Dorado in the quest of new photoCatalysts as photoinitiators of polymerization. *Acc. Chem. Res.* **2016**, *49*, 1980–1989. [CrossRef]
144. Sun, K.; Liu, S.; Chen, H.; Morlet-Savary, F.; Graff, B.; Pigot, C.; Nechab, M.; Xiao, P.; Dumur, F.; Lalevée, J. N-ethylcarbazole-1-allylidene-based push-pull dyes as efficient light harvesting photoinitiators for sunlight induced polymerization. *Eur. Polym. J.* **2021**, *147*, 110331. [CrossRef]
145. Dumur, F. Recent advances on visible light photoinitiators of polymerization based on indane-1,3-dione and related derivatives. *Eur. Polym. J.* **2021**, *143*, 110178. [CrossRef]
146. Abdallah, M.; Bui, T.-T.; Goubard, F.; Theodosopoulou, D.; Dumur, F.; Hijazi, A.; Fouassier, J.-P.; Lalevée, J. Phenothiazine derivatives as photoredox catalysts for cationic and radical photosensitive resins for 3D printing technology and photocomposites synthesis. *Polym. Chem.* **2019**, *10*, 6145–6156. [CrossRef]

147. Abdallah, M.; Hijazi, A.; Graff, B.; Fouassier, J.-P.; Rodeghiero, G.; Gualandi, A.; Dumur, F.; Cozzi, P.G.; Lalevée, J. Coumarin derivatives as high performance visible light photoinitiators/photoredox catalysts for photosensitive resins for 3D printing technology, photopolymerization in water and photocomposites synthesis. *Polym. Chem.* **2019**, *10*, 872–884. [CrossRef]
148. Li, Z.; Zou, X.; Zhu, G.; Liu, X.; Liu, R. Coumarin-Based Oxime Esters: Photobleachable and Versatile Unimolecular Initiators for Acrylate and Thiol-Based Click Photopolymerization under Visible Light-Emitting Diode Light Irradiation. *ACS Appl. Mater. Interf.* **2018**, *10*, 16113–16123. [CrossRef]
149. Abdallah, M.; Dumur, F.; Hijazi, A.; Rodeghiero, G.; Gualandi, A.; Cozzi, P.G.; Lalevée, J. Keto-coumarin scaffold for photo-initiators for 3D printing and photo-composites. *J. Polym. Sci.* **2020**, *58*, 1115–1129. [CrossRef]
150. Abdallah, M.; Hijazi, A.; Dumur, F.; Lalevée, J. Coumarins as powerful photosensitizers for the cationic polymerization of epoxy-silicones under near-UV and visible light and applications for 3D printing technology. *Molecules* **2020**, *25*, 2063. [CrossRef]
151. Chen, Q.; Yang, Q.; Gao, P.; Chi, B.; Nie, J.; He, Y. Photopolymerization of coumarin-containing reversible photoresponsive materials based on wavelength selectivity. *Ind. Eng. Chem. Res.* **2019**, *58*, 2970–2975. [CrossRef]
152. Rahal, M.; Mokbel, H.; Graff, B.; Toufaily, J.; Hamieh, T.; Dumur, F.; Lalevée, J. Mono vs. difunctional coumarin as photoinitiators in photocomposite synthesis and 3D printing. *Catalysts* **2020**, *10*, 1202. [CrossRef]
153. Abdallah, M.; Hijazi, A.; Cozzi, P.G.; Gualandi, A.; Dumur, F.; Lalevée, J. Boron compounds as additives for the cationic polymerization using coumarin derivatives in epoxy-silicones. *Macromol. Chem. Phys.* **2021**, *222*, 2000404. [CrossRef]
154. Guit, J.; Tavares, M.B.L.; Hul, J.; Ye, C.; Loos, K.; Jager, J.; Folkersma, R.; Voet, V.S.D. Photopolymer Resins with Biobased Methacrylates Based on Soybean Oil for Stereolithography. *ACS Appl. Polym. Mater.* **2020**, *2*, 949–957. [CrossRef]
155. Xiao, P.; Dumur, F.; Thirion, D.; Fagour, S.; Vacher, S.; Sallenave, X.; Morlet-Savary, F.; Graff, B.; Fouassier, J.-P.; Gigmes, D.; et al. Multicolor photoinitiators for radical and cationic polymerization: Mono vs. poly functional thiophene derivatives. *Macromolecules* **2013**, *46*, 6786–6793. [CrossRef]
156. Li, J.; Zhang, X.; Ali, S.; Akram, M.Y.; Nie, J.; Zhu, X. The effect of polyethylene glycoldiacrylate complexation on type II photoinitiator and promotion for visible light initiation system. *J. Photochem. Photobiol. A Chem.* **2019**, *384*, 112037. [CrossRef]
157. Li, J.; Li, S.; Li, Y.; Li, R.; Nie, J.; Zhu, X. In situ monitoring of photopolymerization by photoinitiator with luminescence characteristics. *J. Photochem. Photobiol. A Chem.* **2020**, *389*, 112225. [CrossRef]
158. Li, J.; Hao, Y.; Zhong, M.; Tang, L.; Nie, J.; Zhu, X. Synthesis of furan derivative as LED light photoinitiator: One-pot, low usage, photobleaching for light color 3D printing. *Dyes Pigm.* **2019**, *165*, 467–473. [CrossRef]
159. Xu, Y.; Noirbent, G.; Brunel, D.; Ding, Z.; Gigmes, D.; Graff, B.; Xiao, P.; Dumur, F.; Lalevée, J. Novel ketone derivatives based photoinitiating systems for free radical polymerization under mild conditions and 3D printing. *Polym. Chem.* **2020**, *11*, 5767–5777. [CrossRef]
160. Arikawa, H.; Takahashi, H.; Kanie, T.; Ban, S. Effect of various visible light photoinitiators on the polymerization and color of light-activated resins. *Dent. Mater. J.* **2009**, *28*, 454–460. [CrossRef]
161. Tomal, W.; Ortyl, J. Water-Soluble Photoinitiators in Biomedical Applications. *Polymers* **2020**, *12*, 1073. [CrossRef]
162. Tehfe, M.-A.; Dumur, F.; Graff, B.; Clément, J.-L.; Gigmes, D.; Morlet-Savary, F.; Fouassier, J.-P.; Lalevée, J. New Cleavable Photoinitiator Architecture with Huge Molar Extinction Coefficients for Polymerization in the 340−450 nm Range. *Macromolecules* **2013**, *46*, 736–746. [CrossRef]
163. Xiao, P.; Zhang, J.; Dumur, F.; Tehfe, M.-A.; Morlet-Savary, F.; Graff, B.; Gigmes, D.; Fouassier, J.-P.; Lalevée, J. Visible light sensitive photoinitiating systems: Recent progress in cationic and radical photopolymerization reactions under soft conditions. *Prog. Polym. Sci.* **2015**, *41*, 32–66. [CrossRef]
164. Kabatc, J.; Iwinska, K.; Balcerak, A.; Kwiatkowska, D.; Skotnicka, A.; Czechband, Z.; Bartkowiak, M. Onium salts improve the kinetics of photopolymerization of acrylate activated with visible light. *RSC Adv.* **2020**, *10*, 24817–24829. [CrossRef]
165. Crivello, J.V. The Discovery and Development of Onium Salt Cationic Photoinitiators. *J. Polym. Sci. A Polym. Chem.* **1999**, *37*, 4241–4254. [CrossRef]
166. Crivello, J.V.; Lam, J.H.W. Diaryliodonium Salts. A New Class of Photoinitiators for Cationic Polymerization. *Macromolecules* **1977**, *10*, 1307–1315. [CrossRef]
167. Topa, M.; Ortyl, J. Moving Towards a Finer Way of Light-Cured Resin-Based Restorative Dental Materials: Recent Advances in Photoinitiating Systems Based on Iodonium Salts. *Materials* **2020**, *13*, 4093. [CrossRef] [PubMed]
168. Lalevée, J.; Telitel, S.; Xiao, P.; Lepeltier, M.; Dumur, F.; Morlet-Savary, F.; Gigmes, D.; Fouassier, J.-P. Metal and metal free photocatalysts: Mechanistic approach and application as photoinitiators of photopolymerization. *Beilstein J. Org. Chem.* **2014**, *10*, 863–876. [CrossRef]
169. Fouassier, J.-P.; Lalevée, J. Photochemical Production of Interpenetrating Polymer Networks; Simultaneous Initiation of Radical and Cationic Polymerization Reactions. *Polymers* **2014**, *6*, 2588–2610. [CrossRef]
170. Tomal, W.; Chachaj-Brekiesz, A.; Popielarz, R.; Ortyl, J. Multifunctional biphenyl derivatives as photosensitisers in various types of photopolymerization processes, including IPN formation, 3D printing of photocurable multiwalled carbon nanotubes (MWCNTs) fluorescent composites. *RSC Adv.* **2020**, *10*, 32162–32182. [CrossRef]
171. Lalevée, J.; Morlet-Savary, F.; Dietlin, C.; Graff, B.; Fouassier, J.-P. Photochemistry and Radical Chemistry under Low Intensity Visible Light Sources: Application to Photopolymerization Reactions. *Molecules* **2014**, *19*, 15026–15041. [CrossRef]
172. Andrzejewska, E.; Grajek, K. Recent advances in photo-induced free-radical polymerization. *MOJ Poly. Sci.* **2017**, *1*, 58–60. [CrossRef]

173. Corrigan, N.; Shanmugam, S.; Xu, J.; Boyer, C. Photocatalysis in organic and polymer synthesis. *Chem. Soc. Rev.* **2016**, *45*, 6165–6212. [CrossRef]
174. Lalevée, J.; Tehfe, M.-A.; Morlet-Savary, F.; Graff, B.; Dumur, F.; Gigmes, D.; Blanchard, N.; Fouassier, J.-P. Photoredox catalysis for polymerization reactions. *Chimia* **2012**, *66*, 439–441. [CrossRef]
175. Bonardi, A.-H.; Dumur, F.; Noirbent, G.; Lalevée, J.; Gigmes, D. Organometallic vs organic photoredox catalysts for photocuring reactions in the visible region. *Beilstein J. Org. Chem.* **2018**, *14*, 3025–3046. [CrossRef]
176. Banoth, R.K.; Thatikonda, A. A review on natural chalcones an update. *Int. J. Pharm. Sci. Res.* **2020**, *11*, 546–555.
177. Morita, Y.; Takagi, K.; Fukuchi-Mizutani, M.; Ishiguro, K.; Tanaka, Y.; Nitasaka, E.; Nakayama, M.; Saito, N.; Kagami, T.; Hoshino, A.; et al. A chalcone isomerase-like protein enhances flavonoid production and flower pigmentation. *Plant J.* **2014**, *78*, 294–304. [CrossRef]
178. Davies, K.M.; Bloor, S.J.; Spiller, G.B.; Deroles, S.C. Production of yellow colour in flowers: Redirection of flavonoid biosynthesis in Petunia. *Plant J.* **1998**, *13*, 259–266. [CrossRef]
179. Rammohan, A.; Reddy, J.S.; Sravya, G.; Rao, C.N.; Zyryanov, G.V. Chalcone synthesis, properties and medicinal applications: A review. *Environ. Chem. Lett.* **2020**, *18*, 433–458. [CrossRef]
180. Phan, T.P.; Teo, K.Y.; Liu, Z.-Q.; Tsai, J.-K.; Tay, M.G. Application of unsymmetrical bis-chalcone compounds in dye sensitized solar cell. *Chem. Data Coll.* **2019**, *22*, 100256. [CrossRef]
181. Rajakumar, P.; Thirunarayanan, A.; Raja, S.; Ganesan, S.; Maruthamuthu, P. Photophysical properties and dye-sensitized solar cell studies on thiadiazole–triazole–chalcone dendrimers. *Tetrahedron Lett.* **2012**, *53*, 1139–1143. [CrossRef]
182. Sharma, S.; Sharma, A.S.; Agarwal, N.K.; Shahband, P.A.; Shrivastav, P.S. Self-assembled blue-light emitting materials for their liquid crystalline and OLED applications: From a simple molecular design to supramolecular materials. *Mol. Syst. Des. Eng.* **2020**, *5*, 1691–1705. [CrossRef]
183. Zhang, Y.-P.; Wang, B.-X.; Yang, Y.-S.; Liang, C.; Yang, C.; Chai, H.-L. Synthesis and self-assembly of chalcone-based organogels. *Coll. Surf. A* **2019**, *577*, 449–455. [CrossRef]
184. Chen, S.; Qin, C.; Jin, M.; Pan, H.; Wan, D. Novel chalcone derivatives with large conjugation structures as photosensitizers for versatile photopolymerization. *J. Polym. Sci.* **2021**, *59*, 578–593. [CrossRef]
185. Nam, S.W.; Kang, S.H.; Chang, J.Y. Synthesis and Photopolymerization of Photoreactive Mesogens Based on Chalcone. *Macromol. Res.* **2007**, *15*, 74–81. [CrossRef]
186. Yadav, G.D.; Wagh, D.P. Claisen-Schmidt Condensation using Green Catalytic Processes: A Critical Review. *ChemistrySelect* **2020**, *5*, 9059–9085. [CrossRef]
187. Qian, H.; Liu, D. Synthesis of Chalcones via Claisen-Schmidt Reaction Catalyzed by SulfonicAcid-Functional Ionic Liquids. *Ind. Eng. Chem. Res.* **2011**, *50*, 1146–1149. [CrossRef]
188. Rafiee, E.; Rahimi, F. A green approach to the synthesis of chalcones via Claisen-Schmidt condensation reaction using cesium salts of 12-tungstophosphoric acid as a reusable nanocatalyst. *Monatsh. Chem.* **2013**, *144*, 361–367. [CrossRef]
189. Reza Sazegar, M.; Mahmoudian, S.; Mahmoudi, A.; Triwahyono, S.; Abdul Jalil, A.; Mukti, R.R.; Nazirah Kamarudine, N.H.; Ghoreishi, M.K. Catalyzed Claisen–Schmidt reaction by protonated aluminate mesoporous silica nanomaterial focused on the (E)-chalcone synthesis as a biologically active compound. *RSC Adv.* **2016**, *6*, 11023–11031. [CrossRef]
190. Narendera, T.; Venkateswarlu, K.; Vishnu Nayak, B.; Sarkar, S. A new chemical access for 30-acetyl-40-hydroxychalcones usingborontrifluoride–etherate via a regioselective Claisen-Schmidt condensation and its application in the synthesis of chalcone hybrids. *Tetrahedron Lett.* **2011**, *52*, 5794–5798. [CrossRef]
191. Rozmer, Z.; Perjési, P. Naturally occurring chalcones and their biological activities. *Phytochem. Rev.* **2016**, *15*, 87–120. [CrossRef]
192. Shivani, T.; Bhavesh, S. A review: Chemical and biological activity of chalcones with their metal complex. *Asian J. Biomed. Pharmaceut. Sci.* **2020**, *10*, 6–13. [CrossRef]
193. Zhuang, C.; Zhang, W.; Sheng, C.; Zhang, W.; Xing, C.; Miao, Z. Chalcone: A Privileged Structure in Medicinal Chemistry. *Chem. Rev.* **2017**, *117*, 7762–7810. [CrossRef] [PubMed]
194. Singh, P.; Anand, A.; Kumar, V. Recent developments in biological activities of chalcones: A mini review. *Eur. J. Med. Chem.* **2014**, *85*, 758–777. [CrossRef] [PubMed]
195. Jung, J.-C.; Lee, Y.; Min, D.; Jung, M.; Oh, S. Practical Synthesis of Chalcone Derivatives and Their Biological Activities. *Molecules* **2017**, *22*, 1872. [CrossRef] [PubMed]
196. Tehfe, M.-A.; Dumur, F.; Xiao, P.; Delgove, M.; Graff, B.; Gigmes, D.; Fouassier, J.-P.; Lalevée, J. Chalcone derivatives as highly versatile photoinitiators for radical, cationic, thiol-ene and IPN polymerization reactions upon visible lights. *Polym. Chem.* **2014**, *5*, 382–390. [CrossRef]
197. Xu, Y.; Noirbent, G.; Brunel, D.; Liu, F.; Gigmes, D.; Sun, K.; Zhang, Y.; Liu, S.; Morlet-Savary, F.; Xiao, P.; et al. Ketone derivatives as photoinitiators for both radical and cationic photopolymerizations under visible LED and application in 3D printing. *Eur. Polym. J.* **2020**, *132*, 109737. [CrossRef]
198. Gajda, M.; Rybakiewicz, R.; Cieplak, M.; Zołek, T.; Maciejewska, D.; Gilant, E.; Rudzki, P.J.; Grab, K.; Kutner, A.; Borowicza, P.; et al. Low-oxidation-potential thiophene-carbazole monomers for electro-oxidative molecular imprinting: Selective chemosensing of aripiprazole. *Biosens. Bioelectron.* **2020**, *169*, 112589. [CrossRef]
199. Akoudad, S.; Frère, P.; Mercier, N.; Roncali, J. Low Oxidation Potential Tetrathiafulvalene Analogues Based on 3,4-Dialkoxythiophene—Conjugating Spacers. *J. Org. Chem.* **1999**, *64*, 4267–4272. [CrossRef]

200. Czichy, M.; Zhylitskaya, H.; Zassowski, P.; Navakouski, M.; Chulkin, P.; Janasik, P.; Lapkowski, M.; Stępień, M. Electrochemical Polymerization of Pyrrole−Perimidine Hybrids: Low-Band-Gap Materials with High n-Doping Activity. *J. Phys. Chem. C* **2020**, *124*, 14350–14362. [CrossRef]
201. Lee, T.Y.; Guymon, C.A.; Sonny Jönsson, E.; Hoyle, C.E. The effect of monomer structure on oxygen inhibition of (meth)acrylates photopolymerization. *Polymer* **2004**, *45*, 6155–6162. [CrossRef]
202. Belon, C.; Allonas, X.; Croutxé-Barghorn, C.; Lalevée, J. Overcoming the oxygen inhibition in the photopolymerization of acrylates: A study of the beneficial effect of triphenylphosphine. *J. Polym. Sci. A Polym. Chem.* **2010**, *48*, 2462–2469. [CrossRef]
203. Ligon, S.C.; Husár, B.; Wutzel, H.; Holman, R.; Liska, R. Strategies to Reduce Oxygen Inhibition in Photoinduced Polymerization. *Chem. Rev.* **2014**, *114*, 557–589. [CrossRef]
204. Pierrel, J.; Ibrahim, A.; Croutxé-Barghorn, C.; Allonas, X. Effect of the oxygen affected layer in multilayered photopolymers. *Polym. Chem.* **2017**, *8*, 4596–4602. [CrossRef]
205. Lee, J.H.; Prud'homme, R.K.; Aksay, I.A. Cure depth in photopolymerization: Experiments and theory. *J. Mater. Res.* **2001**, *16*, 3536. [CrossRef]
206. Garra, P.; Dietlin, C.; Morlet-Savary, F.; Dumur, F.; Gigmes, D.; Fouassier, J.-P.; Lalevée, J. Photopolymerization of thick films and in shadow areas: A review for the access to composites. *Polym. Chem.* **2017**, *8*, 7088–7101. [CrossRef]
207. Chen, H.; Noirbent, G.; Liu, S.; Zhang, Y.; Sun, K.; Morlet-Savary, F.; Gigmes, D.; Xiao, P.; Dumur, F.; Lalevée, J. In-situ generation of Ag nanoparticles during photopolymerization by using newly developed dyes-based three-component photoinitiating systems and their shape change behavior. *J. Polym. Sci.* **2021**, *59*, 843–859. [CrossRef]
208. Chen, H.; Noirbent, G.; Zhang, Y.; Sun, K.; Liu, S.; Brunel, D.; Gigmes, D.; Graff, B.; Morlet-Savary, F.; Xiao, P.; et al. Photopolymerization and 3D/4D applications using newly developed dyes: Search around the natural chalcone scaffold in photoinitiating systems. *Dyes Pigm.* **2021**, *188*, 109213. [CrossRef]
209. Corakci, B.; Hacioglu, S.O.; Toppare, L.; Bulut, U. Long wavelength photosensitizers in photoinitiated cationic polymerization: The effect of quinoxaline derivatives on photopolymerization. *Polymer* **2013**, *54*, 3182–3187. [CrossRef]
210. Li, J.; Zhang, X.; Nie, J.; Zhu, X. Visible light and water-soluble photoinitiating system based on the charge transfer complex for free radical photopolymerization. *J. Photochem. Photobiol. A Chem.* **2020**, *402*, 112803. [CrossRef]
211. Liska, R. Photoinitiators with functional groups. V. New water-soluble photoinitiators containing carbohydrate residues and copolymerizable derivatives thereof. *J. Polym. Sci. Part A Polym. Chem.* **2002**, *40*, 1504–1518. [CrossRef]
212. Lima, C.G.S.; Lima, T.D.; Duarte, M.; Jurberg, I.D.; Paixao, M.W. Organic synthesis enabled by light-irradiation of eda complexes: Theoretical background and synthetic applications. *ACS Catal.* **2016**, *6*, 1389–1407. [CrossRef]
213. Kaya, K.; Kreutzer, J.; Yagci, Y. A Charge-Transfer Complex of Thioxanthonephenacyl Sulfonium Salt as a Visible-Light Photoinitiator for Free Radical and Cationic Polymerizations. *ChemPhotoChem* **2019**, *3*, 1187–1192. [CrossRef]
214. Wang, D.; Garra, P.; Lakhdar, S.; Graff, B.; Fouassier, J.-P.; Mokbel, H.; Abdallah, M.; Lalevée, J. Charge Transfer Complexes as Dual Thermal and Photochemical Polymerization Initiators for 3D Printing and Composites Synthesis. *ACS Appl. Polym. Mater.* **2019**, *3*, 561–570. [CrossRef]
215. Wang, D.; Kaya, K.; Garra, P.; Fouassier, J.-P.; Graff, B.; Yagci, Y.; Lalevée, J. Sulfonium salt-based charge transfer complexes as dual thermal and photochemical polymerization initiators for composites and 3D printing. *Polym. Chem.* **2019**, *10*, 4690–4698. [CrossRef]
216. Garra, P.; Fouassier, J.-P.; Lakhdar, S.; Yagci, Y.; Lalevée, J. Visible light photoinitiating systems by charge transfer complexes: Photochemistry without dyes. *Prog. Polym. Sci.* **2020**, *107*, 101277. [CrossRef]
217. Tasdelen, M.A.; Lalevée, J.; Yagci, Y. Photoinduced free radical promoted cationic polymerization 40 years after its discovery. *Polym. Chem.* **2020**, *11*, 1111–1121. [CrossRef]
218. Garra, P.; Caron, A.; Al Mousawi, A.; Graff, B.; Morlet-Savary, F.; Dietlin, C.; Yagci, Y.; Fouassier, J.-P.; Lalevée, J. Photochemical, Thermal Free Radical, and Cationic Polymerizations Promoted by Charge Transfer Complexes: Simple Strategy for the Fabrication of Thick Composites. *Macromolecules* **2018**, *51*, 7872–7880. [CrossRef]
219. Zhang, J.; Xiao, P. 3D printing of photopolymers. *Polym. Chem.* **2018**, *9*, 1530–1540. [CrossRef]
220. Baralle, A.; Garra, P.; Graff, B.; Morlet-Savary, F.; Dietlin, C.; Fouassier, J.-P.; Lakhdar, S.; Lalevée, J. Iodinated Polystyrene for Polymeric Charge Transfer Complexes: Toward High-Performance Near-UV and Visible Light Macrophotoinitiators. *Macromolecules* **2019**, *52*, 3448–3453. [CrossRef]
221. Han, W.; Fu, H.; Xue, T.; Liu, T.; Wang, Y.; Wang, T. Facilely prepared blue-green light sensitive curcuminoids with excellent bleaching properties as high performance photosensitizers in cationic and free radical photopolymerization. *Polym. Chem.* **2018**, *9*, 1787–1798. [CrossRef]
222. Ebner, C.; Mitterer, J.; Eigruber, P.; Stieger, S.; Riess, G.; Kern, W. Ultra-High Through-Cure of (Meth)Acrylate Copolymers via Photofrontal Polymerization. *Polymers* **2020**, *12*, 1291. [CrossRef] [PubMed]
223. Zhou, X.; Soppera, O.; Plain, J.; Jradi, S.; Sun, X.W.; Demir, H.V.; Yang, X.; Deeb, C.; Gray, S.K.; Wiederrecht, G.P. Plasmon-based photopolymerization: Near-field probing, advanced photonic nanostructures and nanophotochemistry. *J. Opt.* **2014**, *16*, 114002. [CrossRef]
224. Chen, H.; Noirbent, G.; Zhang, Y.; Brunel, D.; Gigmes, D.; Liu, S.; Sun, K.; Morlet-Savary, F.; Graff, B.; Xiao, P.; et al. Novel D-π-A and A-π-D-π-A three-component photoinitiating systems based on carbazole/triphenylamino based chalcones and application in 3D and 4D Printing. *Polym. Chem.* **2020**, *11*, 6512–6528. [CrossRef]

225. Jeong, H.Y.; Woo, B.H.; Kim, N.; Jun, Y.C. Multicolor 4D printing of shape-memory polymers for light-induced selective heating and remote actuation. *Sci. Rep.* **2020**, *10*, 6258. [CrossRef]
226. Bajpai, A.; Baigent, A.; Raghav, S.; Brádaigh, C.O.; Koutsos, V.; Radacsi, N. 4D Printing: Materials, Technologies, and Future Applications in the Biomedical Field. *Sustainability* **2020**, *12*, 10628. [CrossRef]
227. Chu, H.; Yang, W.; Sun, L.; Cai, S.; Yang, R.; Liang, W.; Yu, H.; Liu, L. 4D Printing: A Review on Recent Progresses. *Micromachines* **2020**, *11*, 796. [CrossRef]
228. Lee, A.Y.; An, J.; Chua, C.K. Two-Way 4D Printing: A Review on the Reversibility of 3D-Printed Shape Memory Materials. *Engineering* **2017**, *3*, 663–674. [CrossRef]
229. Keneth, E.S.; Lieberman, R.; Rednor, M.; Scalet, G.; Auricchio, F.; Magdassi, S. Multi-Material 3D Printed Shape Memory Polymer with Tunable Melting and Glass Transition Temperature Activated by Heat or Light. *Polymers* **2020**, *12*, 710. [CrossRef]
230. Yuan, C.; Wang, F.; Ge, Q. Multimaterial direct 4D printing of high stiffness structures with large bending curvature. *Ext. Mech. Lett.* **2021**, *42*, 10112.
231. Zhang, Y.; Zhang, Y.; Josien, L.; Salomon, J.-P.; Simon-Masseron, A.; Lalevée, J. Photopolymerization of Zeolite/Polymer-Based Composites: Toward 3D and 4D Printing Applications. *ACS Appl. Polym. Mater.* **2021**, *3*, 400–409. [CrossRef]
232. Inverardi, N.; Pandini, S.; Bignotti, F.; Scalet, G.; Marconi, S.; Auricchio, F. Sequential Motion of 4D Printed Photopolymers with Broad Glass Transition. *Macromol. Mater. Eng.* **2020**, *305*, 1900370. [CrossRef]